12-2018

Generation of 360 Degree Point Cloud for Characterization of Morphological and Chemical Properties of Maize and Sorghum

Suresh Thapa
University of Nebraska - Lincoln, suresh.thapa@huskers.unl.edu

GENERATION OF 360 DEGREE POINT CLOUD FOR CHARACTERIZATION OF MORPHOLOGICAL AND CHEMICAL PROPERTIES OF MAIZE AND SORGHUM

by

Suresh Thapa

A THESIS

Presented to the Faculty of

The Graduate College at the University of Nebraska

In Partial Fulfilment of Requirements

For the Degree of Master of Science

Major: Agricultural and Biological Systems Engineering

Under the Supervision of Professor Yufeng Ge

Lincoln, Nebraska

December, 2018

GENERATION OF 360 DEGREE POINT CLOUD FOR CHARACTERIZATION OF MORPHOLOGICAL AND CHEMICAL PROPERTIES OF MAIZE AND SORGHUM

Suresh Thapa, M.S.

University of Nebraska, 2018

Advisor: Yufeng Ge

Recently, imaged-based high-throughput phenotyping methods have gained popularity in plant phenotyping. Imaging projects the 3D space into a 2D grid causing the loss of depth information and thus causes the retrieval of plant morphological traits challenging. In this study, LiDAR was used along with a turntable to generate a 360-degree point cloud of single plants. A LABVIEW program was developed to control and synchronize both the devices. A data processing pipeline was built to recover the digital surface models of the plants. The system was tested with maize and sorghum plants to derive the morphological properties including leaf area, leaf angle and leaf angular distribution. The results showed a high correlation between the manual measurement and the LiDAR measurements of the leaf area (R^2>0.91). Also, Structure from Motion (SFM) was used to generate 3D spectral point clouds of single plants at different narrow spectral bands using 2D images acquired by moving the camera completely around the plants. Seven narrow band (band width of 10 nm) optical filters, with center wavelengths at 530 nm, 570 nm, 660 nm, 680 nm, 720 nm, 770 nm and 970 nm were used to obtain the images for generating a spectral point cloud. The possibility of deriving the biochemical properties of the plants: nitrogen, phosphorous, potassium and moisture content using the multispectral information from the 3D point cloud was tested through statistical modeling techniques. The results were optimistic and thus indicated the possibility of generating a 3D spectral point cloud for deriving both the morphological and biochemical properties of the plants in the future.

Keywords: high-throughput plant phenotyping, leaf area, leaf angle, leaf angular distribution, 3D point cloud, LiDAR, structure from motion, spectral point cloud.

ACKNOWLEDGMENTS

I would like to express my heartfelt gratitude towards my advisor Dr. Yufeng Ge who has always been a friendly mentor and has supported my study and research continuously with great patience. He is truly a source of inspiration, who has motivated me when I was feeling low and guided me through the difficult times during work and study.

I am also very grateful to my thesis committee members Dr. Harkamal Walia and Dr. Hongfeng Yu for their very helpful comments and suggestions. I would also like to thank Feiyu Zhu for his invaluable help in point cloud data processing.

During the last two years at UNL, friends have become a family away from home. I sincerely thank Piyush Pandey, Nuwan Wijewardane, Abbas Atefi, Geng Bai, Ujjwol Bhandari and Wenan Yuan for being through thick and thin with me. I am also very thankful to Vincet Stoerger and Troy Pabst for their kind help in conducting experiments at phenotyping greenhouse facility on UNL's Innovation Campus. I also acknowledge National Science Foundation (DBI-1556186) for providing funding for this research.

I finally thank my parents and my younger brother for their unconditional love and support throughout my life.

TABLE OF CONTENTS

LIST OF FIGURES

LIST OF TABLES

CHAPTER 1

INTRODUCTION

1.1 PLANT BREEDING AND PHENOTYPING

"Plant Breeding is the art and science of changing the traits of plants in order to produce desired characteristics" (Poehlman, Sleper, and Rudd, 1995). Plant breeder's job is to produce a desirable variety by selecting the suitable traits and removing the unwanted ones from a large population. For making these decisions, they need to rely on knowledge of both genotype and phenotype. Nowadays, there are advanced genotyping techniques with high speed and accuracy for selecting genes for a trait. The advancements in high throughput sequencing have greatly reduced the cost for genotyping and at the same time improved the efficiency of plant breeding in last few decades (Duran et al., 2009). However, methods for generating phenotype data are still labor intensive, time consuming and generally involves manual measurements in fields which are prone to errors. Moreover, data collected are poor in temporal and spatial resolution and lack the throughput to match with the genotyping speed. Hence, phenotyping has become a bottleneck in plant breeding.

A phenotype is a combination of any observable characteristics in an organism especially those traits that can be measured and is a result of the genotype, environmental effects and, their interactions. One of the most important objectives of plant phenotyping is to select the better variety which has higher yield and to enhance other essential characteristics like nutrient quality, resistance against diseases & pests, tolerance to weather conditions like drought, wind & salinity, efficiency in resource uses, and ease of cultivation, harvesting and processing (Fiorani and Schurr, 2013). One of the jobs of the plant breeder is to measure the phenotypes such that traits with desirable characteristics

can be chosen. For example, one of the simplest methods of selection might be a visual inspection with a human eye for traits such as fruit color/shape. However, for other traits such as abundance of a certain nutrient in a fruit, more complex and time-consuming measurement needs to be done for maximizing the accuracy of selection. Such measurements take a lot of effort and are usually destructive. Even if the measurement is as simple as measuring the plant height, it becomes a great pain when there are thousands of plants to be measured manually. Thus, research in phenotyping is essential to address these challenges, particularly in plant breeding (Passioura, 2012).

High throughput plant phenotyping (HTPP) techniques have emerged to be a promising tool to solve these problems. In recent years, there have been a burst of phenotyping facilities with automated sensing and data collection technologies for monitoring plant growth. Such facilities are equipped with different types of imaging modules that can capture images of hundreds of plants per day.

Image-based approaches to rapidly and nondestructively measure plant morphological traits have emerged and quickly developed in response to the need for accelerating high-throughput plant phenotyping that would eventually enable effective use of genomic data to bridge the genotype-to-phenotype gap for crop improvement (Fahlgren, Gehan, and Baxter, 2015; Furbank and Tester, 2011). Image analysis has been used successfully to measure the physical traits of plant shoots including height, leaf area, and biomass (M. T. Campbell et al., 2015; Fahlgren et al., 2015; Ge, Bai, Stoerger, and Schnable, 2016). More importantly, by combining information from a series of plant images over time, it has become feasible to capture dynamic traits, such as growth rate, rate of senescence, and estimation of plant architecture. The approaches that involve quantifiable dynamic traits have the potential to significantly impact targeted crop research for increased stress tolerance as stress responses in plants are highly dynamic.

Although image-based approaches have been applied to measure plant structures in 3D, it has intrinsic limitations. Because imaging projects a 3D object onto a 2D image plane, the

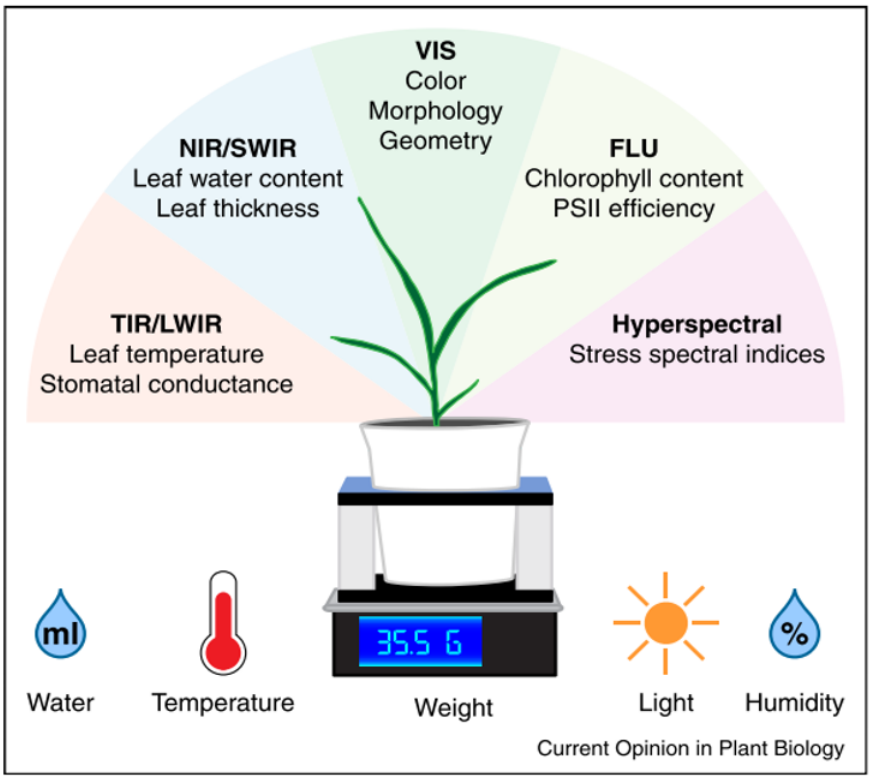

Figure 1.1. High throughput phenotyping platforms collect different types of images to predict respective properties and, also collect other environmental data like water supply, temperature, light, and humidity (Source: Fahlgren, Gehan, and Baxter, 2015).

depth information is lost. This in turn causes an occlusion problem, where part of the plant is not visible in a specific image. To infer the total leaf area or biomass from the projected leaf areas, empirical relationships are usually developed from multi-view images (usually two to three side views and one top view (Klukas, Chen, and Pape, 2014). However, such relationships are usually species dependent and may not be applied broadly to a range of plant species or growth stages.

1.2 NEED FOR 3-DIMENSIONAL MODELLING OF PLANT

It is obvious that plant morphological parameters can be more accurately measured in 3D. Accurate measurement of the 3D structure of a plant is important for enhancing the study of plant phenomics. The 3D structure (shape, size, angle, number, etc.) of leaves affects the physiological processes of the plant. For example, plant leaf area and angle significantly influence light interception and apparent transpiration, photosynthesis, and plant productivity (Goudriaan and Laar, 2012). Processes like carbon uptake and assimilation, emission of volatile organic compounds, element deposition, inception of rain, evaporation etc. are also dependent in the surface area of the canopy.

One particular use of a three-dimensional model of a plant is in creating a Functional Structural Plant Model (FSPM) to understand the plant morphology from a mathematical perspective. FSPM is a holistic approach towards plant modelling and combines the 3D structure of the plant with the simulation of one or many physiological processes. After the availability of powerful computers, the combination of the complex functional models and geometric models into a complete plant have become possible and such models are also called ‘virtual plants’ (Hanan, 1997). FSPM considers that the adaptation of plants to environment is not only by altering the physiological functions like photosynthesis & transpiration but also by changing their structure (e.g. shedding of leaves, shape & orientation of leaves) (Vos et al., 2010). In other words, plant morphology and physiology are interdependent and the 3D information about morphology is vital in simulating

physiological processes like photosynthesis and transpiration (Larcher, 2003).

Sinoquet, Le Roux, Adam, Ameglio, and Daudet (2001) modelled the spatial distribution of radiation absorption, transpiration and photosynthesis using 3D representation of the canopy, combined with environmental factors and physiological leaf properties. Dauzat, Rapidel, and Berger (2001) used the virtual plants for simulating leaf transpiration and sap flow in coffee plants. Virtual plant models have been used in a number of research studies and thus demonstrates the importance of the need for 3D modelling of plants (Robert, Fournier, Andrieu, and Ney, 2008; Tardieu, 2003; Wilson and Chakrabrty, 1998). Another example for the application of 3D modelling is in determining the optimal volume of pesticides to be applied, for instance in tomato plants as shown by (Campolide, 2007). The rate and volume of chemicals to be applied is related to the 3D canopies and the canopy Leaf Area Index (LAI)(Furness, Magarey, Miller, and Drew, 1998; Siegfried, Viret, Huber, and Wohlhauser, 2007). LAI is the leaf area per unit ground surface cover.

1.3 TECHNIQUES FOR 3-DIMENSIONAL MODELLING OF PLANTS

Many existing 3D modelling techniques are used for the reconstruction of man-made objects which usually have simpler geometry, less occlusion and are rich in texture. However, plants pose relatively complex and dynamic geometry and reconstructing their 3D model is a challenging problem. Figure 1.2 provides an overview of the existing 3D reconstruction techniques for plants and can be mainly divided into active and passive methods. Passive sensors gather the information by capturing the default radiation present in the environment in which the object lies. Regular RGB cameras are one of the most common passive sensors used these days. On the other hand, active sensors have their own source of illumination, which includes a transmitter to send out a signal and a receiver to detect the reflected signal. LiDAR is an example of active sensor.

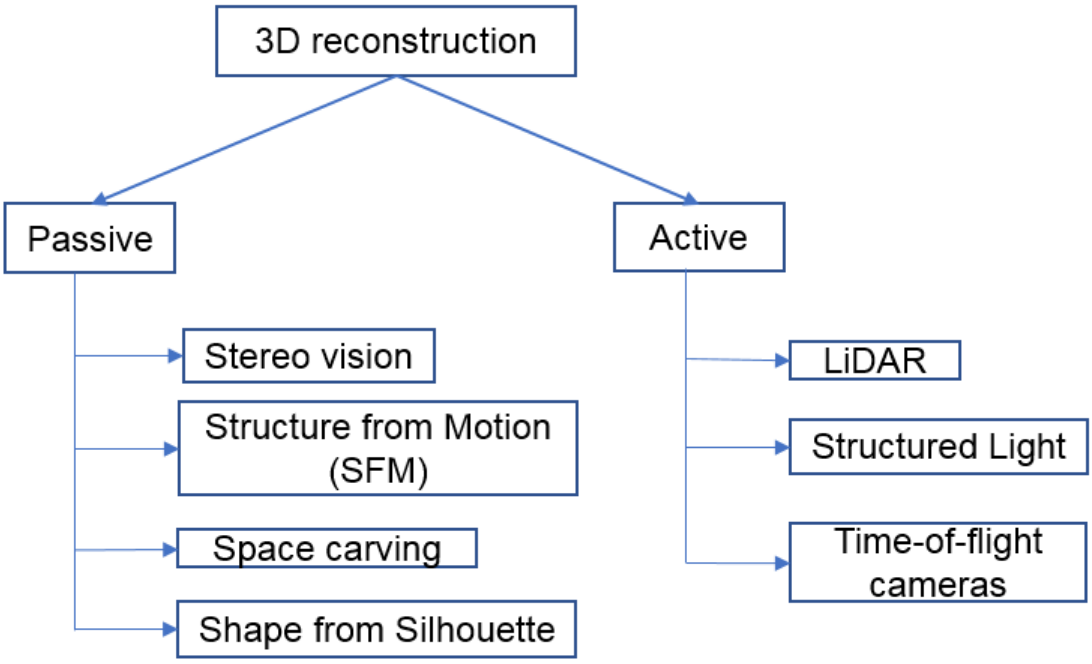

Figure 1.2. Three-dimensional reconstruction techniques

1.3.1 PASSIVE METHODS

Stereo vision is the principle of finding the depth information from two or more 2D images. The difference in the pixel position in the two images of the same 3D point gives the depth value. In order to identify the pixels in the images that represent the same point in the real world, they must be matched, and this process is called correspondence. Correspondence is a 2D search problem which is converted into a 1D search by rectifying the images using the internal and external camera parameters obtained through camera calibration. After the identical pixels are located in the two images, the shift in their position is calculated which is known as the disparity and is used to calculate the depth value of the pixels. Disparity is inversely proportional to depth i.e. disparity will be higher for nearer objects and lower for farther objects.

Biskup, Scharr, Schurr, and Rascher (2007) presented a binocular stereo vision system that can be used to create a partial 3D model of the outer canopy and used those models to

study the diurnal variations in leaf angle of soybean canopy. T. T. Nguyen, Slaughter, Max, Maloof, and Sinha (2015) used a combination of 10 RGB cameras to take the picture of the scene illuminated by the LED arrays which were used for enhancing the texture of the object. The light patterns also helped to perform better in stereo matching of the pixels in the images. The accuracy of stereo imaging depends on the ability to match the corresponding points in the image pair to gain the depth information, which can be sensitive to environmental conditions, ineffective for low texture scenes, and computationally intensive for large images (Li, Zhang, and Huang, 2014).

Structure from motion (SFM) is another technique similar to stereo vision in which the 3D structure is obtained by the information from numerous images taken by a camera moving around the object. This technique is discussed more in detail in Chapter 3.

Space carving is another 3D reconstruction technique that uses images from multiple views. The object is photographed from several cameras placed around it such that the object totally lies in the image. A binary mask, which is the projection of the object from a certain view, is extracted. All these binary masks are projected into a solid cube that can bound the object according to their angle of views. After each of the projection, the part of the cube that does not belong to the object are carved away. Finally, after adding all the images, only the part in the cube that belongs to the object is left behind. Kumar, Cai, and Miklavcic (2013)) studied the root system architecture of corn seedlings grown in a transparent gel-based medium. The observations were made with digital cameras and then the 3D reconstruction of the roots was done using space carving algorithms.

Shape-From-Silhouette (SFS) is another type of 3D reconstruction method which constructs a 3D shape estimate of an object using silhouette images of the object. A silhouette is a binary image and can be obtained by segmentation techniques. Then, using the camera parameters, a 3D volumetric model is obtained from the intersection of all the binary silhouettes projected into 3D. The resulting model is called a convex hull. The advantage of this method is that the visual hull entirely depends on the silhouette and is

therefore independent of the object appearance, illumination variation, contrasting pixels and presence of textured regions (Mikhnevich and Hébert, 2011). On the other hand, the main disadvantage of visual hull is its inability to obtain the exact shape of the object. Golbach, Kootstra, Damjanovic, Otten, and van de Zedde (2016) used this technique for 3D reconstruction of seedlings and validated the measurement of plant volume, leaf area and stem length. C. V. Nguyen et al. (2016) also used the 3D visual hull reconstruction algorithm on plastic models of different plants and evaluated the performance for geometric measurements.

1.3.2 ACTIVE METHODS

Time-of-Flight (ToF) cameras or also called depth cameras calculate the distance to the target by measuring the time of flight between emission and reception of the light signal. These types of cameras produce the depth image which means that each pixel in the image also has a distance value of the corresponding point in the scene. When a large number of plants have to be scanned, the 3D point cloud acquisition becomes time consuming and generates a huge volume of data. In some situations, complete 3D reconstruction of the plants may not be necessary for example when morphology of only the canopy structure is needed. Time of flight cameras prove to be very effective in these cases as they can get the depth information of the entire scene at once without scanning line by line as in case of LiDARs. However, similar to other methods, as no technique is perfect, there are some limitations to Time-of-flight cameras too. There are problems of low depth precision, low spatial resolution as well as other errors caused by radiometric, geometric and illumination variations.

Alenyà, Dellen, and Torras (2011) used high-resolution color data obtained from calibrated RGB camera and combined it with sparse depth information provided by a ToF camera for the 3D modelling of leaves. Some more applications of the ToF 3D data acquisition technique can be found in following articles (Glasbey, Polder, Heijden, and

Table 1.1. Comparison of the current 3-dimensional reconstruction techniques for plants (Liu, Acosta-Gamboa, Huang, and Lorence, 2017)

System	Principle	Advantages	Disadvantages
Stereo Vision	This technique uses two cameras to capture the same target and derives depth information from those images.	• Inexpensive system • Color information is available	• Sensitive to lighting conditions • Poor depth resolution • High computation power
SFM	Sequence of images are captured by moving a camera around the object to create a three-dimensional model.	• Suitable for complex geometry of plants and can solve occlusion given suitable number of images including numerous views	• High computation required
Space carving	The 2D images are projected in a 3D space (cube) and the voxels from the cube that do not belong to the object are removed to get the 3D model of the object.	• Fast image acquisition as multiple cameras are used to take the images at a time from different positions • Color information can be obtained	• Good imaging setup is required often requiring a homogeneous illumination and clear background • Expensive as multiple cameras are required
Shape from Silhouette	Constructs a 3D shape estimate (convex hull) of the object using the silhouette images.	• Easy to implement and use • Independent of illumination and texture of the object	• Only approximates the shape of an object and does not give the true dimensions
Time-of-Flight cameras	The depth value of every pixel in the image is obtained from the time of flight principle.	• Fast acquisition	• Poor XY resolution • Poor depth resolution • Sensitive to lighting conditions
Structured light	Depth information is calculated by measuring the shift of the projected light (usually from laser) patterns in the images of the plants taken by obtained from a camera.	• Inexpensive system • Color information is available	• Poor XY resolution • Poor depth resolution • Susceptible to sunlight
LiDAR	It calculates the distance to target in real time by measuring the time of flight.	• Accurate and fast • Less sensitive to ambient lighting • High scanning range	• Bad edge detection • Expensive

Song, 2014a; Kazmi, Foix, Alenyà, and Andersen, 2014; Mccormick, Truong, and Mullet, 2016).

A structured light 3D scanner is also an active sensing technology for measuring the 3D structure of an object and uses a combination of light patterns and a camera to do so. A light source (usually laser light) is projected into the scene and its image is captured by a camera. If the scene is a planar surface without any depth variation, the light pattern in the image is similar to that of the projected illumination pattern in the scene. However, when there is an uneven depth in the scene, the light patterns are distorted in the image taken by the camera. After the calibration of the system, accurate 3D geometry can be recovered based on the information from the distortion of the structured light pattern. The triangulation of the camera, light source and the object is the principle behind the recovery of the depth information. The light patterns used in this method includes spots, lines or even 2D grids. A very popular device working under this principle is the Microsoft Kinect which projects a rectangular infrared dot pattern on the objects to obtain the depth information (Chen, Zhang, Yan, Li, and Zhou, 2012; Chéné et al., 2012; Jiang, Li, and Paterson, 2016). Azzari, Goulden, and Rusu (2013) used the Microsoft Kinect to measure the vegetation structure including base diameter, height and volume. Yamamoto et al. (2013) used this sensor to monitor the growth of strawberry plant. Paulus, Behmann, Mahlein, Plümer, and Kuhlmann (2014) used and compared several 3D sensors including Kinect to measure the geometry of plants.

The advantage of these types of system is their low cost and the ability to obtain the color images in addition to the depth information. However, such systems are less flexible as they are calibrated only for a fixed range which is usually small. The light patterns can be easily overexposed by the sunlight or other artificial lighting systems in the greenhouse. Therefore, this method only works best when scanning in the night time or in closed imaging chambers. The X-Y resolution of the system is limited by the resolution of the camera. Normally, infrared lighting is used in these systems and infrared detectors

usually have lower resolution compared to the visible cameras.

LiDAR is another very popular active sensing method which is discussed in detail in Chapter 2.

1.4 OBJECTIVES OF THE STUDY

There are two main objectives of this study. The first objective is to generate a 3D point cloud of maize and sorghum plants and derive the morphological parameters of those plants. The morphological parameters to be computed from the point 3D point clouds are leaf area, leaf angle and leaf angular distribution.

The second objective is to generate a 3D point cloud of maize plant such that the 3D points not only contain the spatial information but also the spectral information. This leads us to another objective of finding whether the chemical properties (Nitrogen, Phosphorous and Potassium) and water content of leaves can be inferred from the 3D spectral point cloud.

CHAPTER 2

GENERATION OF 3D POINT CLOUD USING LIDAR TO MEASURE MORPHOLOGICAL PROPERTIES OF MAIZE AND SORGHUM

2.1 BACKGROUND

2.1.1 LiDAR IN PLANT PHENOTYPING

LiDAR (Light Detection and Ranging) employs the time-of-flight principle of active lasers to acquire 3D information of an object (Figure 2.1). LiDAR was originally developed for terrain, benthic and forest surveys from aerial platforms (Wehr and Lohr, 1999). Later on, terrestrial LiDAR scanning (TLS) systems were developed and used to measure the 3D structural properties of buildings, bridges, and trees. More recently, the applications of TLS systems in agriculture have also been reported. For example, Eitel, Magney, Vierling, Brown, and Huggins (2014) demonstrated the feasibility of a green TLS to measure dry biomass and the nitrogen concentration of winter wheat crops. Friedli et al. (2016) showed that a 3D TLS allowed for the measurement of canopy height growth of maize, soybean, and wheat with high temporal resolution. More recently, LiDAR sensors were mounted on mobile platforms to measure height and above ground biomass of field grown crops (Jimenez-Berni et al., 2018; Madec et al., 2017; Sun, Li, and Paterson, 2017).

Because of its capability to measure structure and shape in 3D and because of the decrease in its price with the advancement in technology, LiDAR is regarded as an important technology to complement 2D image analysis for high-throughput plant phenotyping (Lin, 2015). It would be particularly useful to measure the structural and morphological properties of plant shoots such as leaf area and leaf orientation. These parameters are most accurately quantified in 3D space, and it is a challenging task to

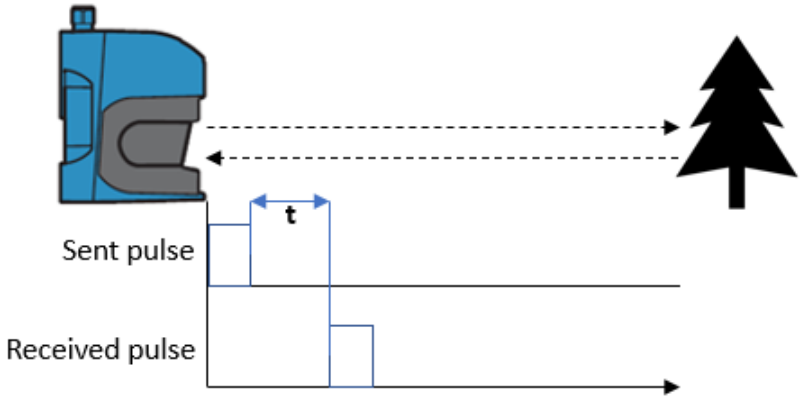

Figure 2.1. Principle of Time-of-flight measurement

reconstruct them from a set of 2D images. Paulus, Schumann, Kuhlmann, and Léon (2014) used a precision laser scanning device (a LiDAR based on continuous wave phase modulation) coupled to an articulated measuring arm to generate 3D point clouds of barley (Hordeum vulgare L.) plants. They showed that traits, including leaf area and stem height, could be quantified through the processing of LiDAR point clouds. This study clearly demonstrated the usefulness of LiDAR to measure the structural parameters of single plants. However, the use of an articulated arm to direct the laser beam onto the plant surface involved a manual process. To measure larger plants, such as maize or sorghum, the measurement time would also be significantly longer. Because of the strong need to link genotype to phenotype, automated and faster approaches are needed to increase the throughput and flexibility of a LiDAR based system.

2.1.2 LEAF AREA, LEAF ANGLE AND LEAF ANGULAR DISTRIBUTION

As discussed earlier, Leaf area is a powerful indication of plant productivity. Leaf area is a highly dynamic trait which varies with temperature, rainfall, irradiation level and various

other local environmental factors (Nicotra et al., 2011). Higher water use efficiency was associated with lower leaf water content (LWC) and specific leaf area (SLA) (Lu et al., 2012). Traditional techniques available for measuring leaf area are laborious, time consuming and usually destructive. One of the earliest methods is to trace the outline of the leaves on a paper and calculate the area from it (Miller, 1938). Some other procedures include allometric models and equations to convert the leaf length and width to the leaf area (Stewart and Dwyer, 1999). Glasbey, Polder, Heijden, and Song (2014b) used combination of stereo and Time-of-Flight (ToF) images for non-destructive measurement of leaf area. ImageJ is one of the widely used image-based software that is used to calculate projected leaf area by threshold based pixel count (Carins Murphy, Jordan, and Brodribb, 2012; Juneau and Tarasoff, 2012; Warman, Moles, and Edwards, 2011). Similarly, Easy Leaf Area is another such software which calculates leaf area from digital images (Easlon and Bloom, 2014). Although these tools are simple and straightforward to use, they give only an approximation of leaf area and do not account leaf overlap and occlusion.

Leaf area must be considered along with the leaf angle to derive their net impact on the photosynthetic efficiency of the plant. Further, leaf angle is an important determinant of optimal planting density in many crops. Manual measurement of leaf angle involves the procedure of aligning an inclinometer with each leaf segment on a plant (Jones and Vaughan, 2010). Obviously, these methods are not suitable to measure hundreds of plants continuously in a modern plant phenotyping setting that requires rapid and nondestructive assays.

Leaf positioning is very important architectural trait in the plants with respect to adaptation of the plant to its environment. Leaf angles in some plants may be fixed without showing any variation to the dynamic surrounding conditions. On the contrary, in several species, leaves within a plant canopy are also constantly changing their orientation to optimize themselves to the availability of resources like water and radiation as well as

to avoid detrimental conditions like heat stress, wind stress etc. (Zanten, Pons, Janssen, Voesenek, and Peeters, 2010).

De Wit (1965) grouped the plant canopies into four different categories according to their accumulative frequency of leaf angle occurrence as shown in Figure 2.2. Horizontal leaves are most frequent in planophile distribution whereas vertical leaves are most abundant in erectophile distribution. In the plagiophile canopies, oblique inclinations are most frequent and the same are least frequent in the extremophile canopies.

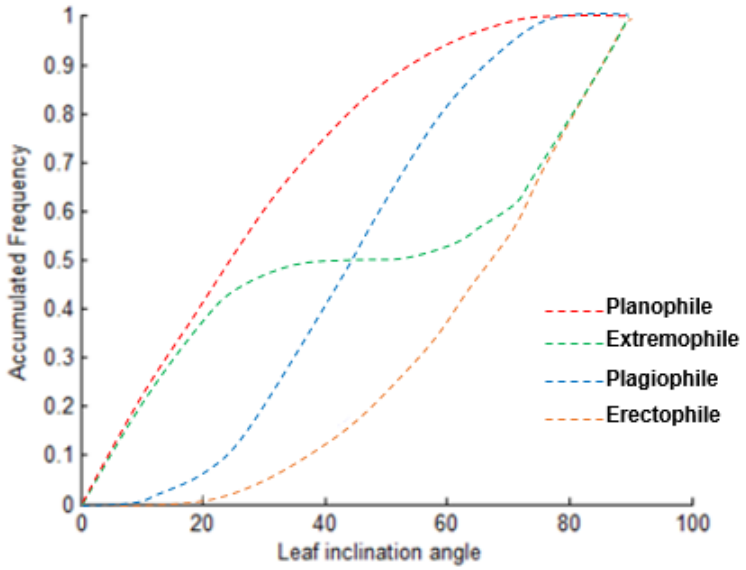

Figure 2.2. Accumulative frequency of four type of canopy proposed by De Wit, 1965 (Source : Fang, 2015)

Planophile canopies capture most light in the upper layers of the canopy but cause a significant shading in the lower layers of leaves. Thus, leaf angles are one of the important factors for the distribution of light in a canopy (Goudriaan, 1988; Hirose, 2005). Erectophile canopies have lower extinction coefficient and consequently cause more uniform distribution of radiation over the leaves compared to planophile canopy

distribution. This increases the overall carbon gain at the whole canopy level as leaves lower in the canopy can contribute more without significantly affecting the photosynthesis rate of upper leaves.

A vertical orientation of leaves can also help to reduce the radiation load at midday. Horizontal leaves usually absorb large amount of radiation which might result in a substantial rise of leaf temperature above the air temperature (Pons, Lambers, and Chapin III, 1998). High leaf temperatures may not be optimal for photosynthesis. Also, the transpiration rate goes up and consequently the water use efficiency of the plant decreases. As a result, the species that have a limited capacity of dealing with high radiation stress may cope with it by adjusting their leaf angles. Moreover, such adjustment of leaf angles may not only be to avoid high radiation but a response to other adverse environmental conditions like shading and complete submergence (Zanten et al., 2010).

Structure of the canopy not only affects the basic functioning of the plant but by doing so, ultimately affects the yield too. For example, the introduction of a new rice cultivar with more vertical leaf orientation contributed to increased rice productivity (Nobel, Forseth, and Long, 1993). Field investigations of the relationships between leaf angle and grain yield and apparent photosynthesis suggested higher grain yields for the hybrid with erect leaves than its counterpart with horizontal type leaves (Pendleton, Smith, Winter, and Johnston, 1968).

Breeding techniques and/or genetic modification can be used to design the canopy structure within some limits (Reynolds, van Ginkel, and Ribaut, 2000) and the better quantitative knowledge of a canopy structure would help to further enhance such efforts.

This chapter describes the development of a novel LiDAR-based sensing system that can automatically produce 3D point clouds of plants with a 360-degree. Also, a data processing pipeline to reconstruct plant leaf surfaces and derive leaf area, leaf inclination angle, and leaf angular distribution is developed. The performance of the instrument is validated on two agronomically and economically important crop species: maize and

sorghum. In addition, relationship between the plant biomass and total surface area of plants is also observed.

2.2 MATERIALS AND METHODS

2.2.1 DESCRIPTION OF HARDWARE AND SOFTWARE OF THE INSTRUMENT

The physical setup of the instrument is shown in Figure 2.3(A). The plant is placed on a rotation stage to provide continuous rotation at 360°. A LiDAR emits laser beams that scan vertically to cover the height of the plant. The combination of the rotating and scanning motion allows for the creation of the 3D point cloud of the plant with a 360° view.

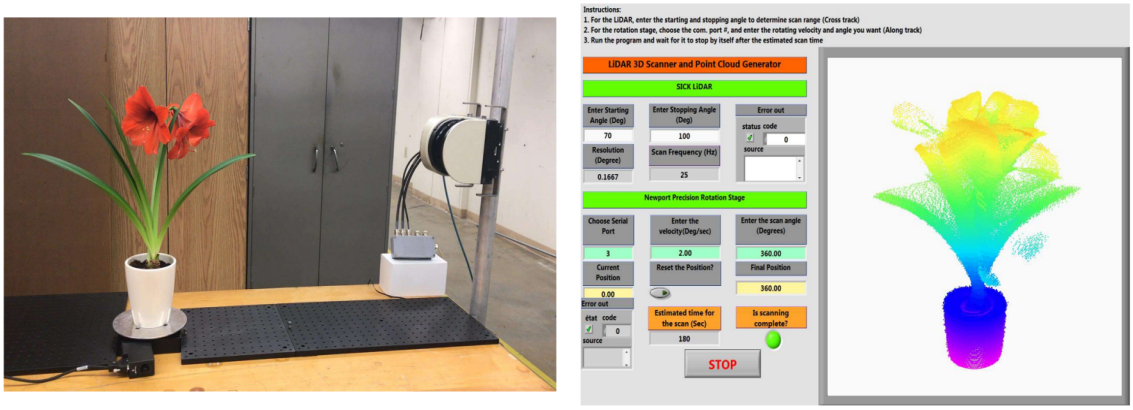

Figure 2.3. Illustration of the new instrument consisting of a LiDAR scanner and precision rotation stage for 3D measurement of plants at 360° view (A). The LabVIEW graphic user interface for instrument control, measurement acquisition, and real-time point cloud visualization (B) (Source: Thapa, Zhu, Walia, Yu, and Ge, 2018).

2.2.1.1 LiDAR

An off-the-shelf LiDAR module (LMS 511, SICK AG) was selected for instrument development. The LMS 511 operates on a time-of-flight principle to calculate the distance to a target. It uses an NIR laser diode (at 905 nm) to send out pulsed laser beams, which

are then reflected from the target and received by the laser detector. Because vegetation normally has higher reflectivity in the NIR spectral range, this increases the detection and ranging accuracy of reflected laser energy. This instrument has an adjustable scanning frequency between 25 Hz and 100 Hz. At 25 Hz, the angular interval of the laser beam is 0.0029 radian. The plant is placed approximately 1.0 to 1.5 m from the LiDAR scanner. This translates to 2.9 to 4.4 mm of sampling resolution of the point cloud along the vertical scanning direction. In addition, the LiDAR has a ranging precision of 6 mm. The LiDAR connects to the computer via an Ethernet connection and data packets are transmitted using a User Datagram Protocol.

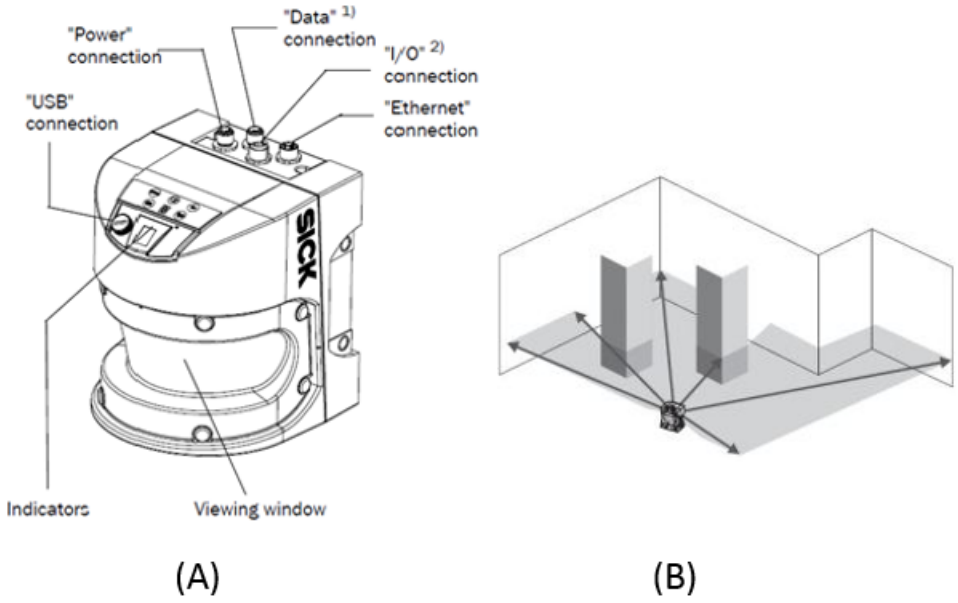

Figure 2.4. (A) SICK LMS 511 LiDAR (B) Scanning range of LiDAR - It has 190-degree FOV and scans in a 2D plane (Source: SICK Operating Manual)

A data packet sent by the LiDAR is in the following string format.

sRN LMDscandata sRA LMDscandata 0 1 9E14CE 0 0 ECF8 ED6E C267B795

Table 2.1. Features of SICK LMS511 LiDAR

Wavelength	905 nm (invisible infrared light)
Field of View	Maximum 190 degree
Pulse output	29.6 W
Pulse duration	2.9 ns
Angular resolution	0.1667/ 0.25/ 0.3333/ 0.5/ 0.6667/ 1 degree
Scanning frequency	25/ 35/ 50/ 75/ 100 Hz
Data interface	Ethernet, RS-232, USB
Scanning range	Scanning range up to 80 m with (100 % object remission (26 m with 10 % object remission)

C268A7A8 0 0 3F 0 0 9C4 21C 1 3AD 0 5 DIST1 3F800000 00000000 DBBA0 683 1F 0 0 0 0 890B 8927 DIST2 3F800000 00000000 DBBA0 683 1F 0 0 0 0 0 0 DIST3 3F800000 00000000 DBBA0 683 1F 0 0 0 0 0 0 DIST4 3F800000 00000000 DBBA0 683 1F 0 0 0 0 0 0 DIST5 3F800000 00000000 DBBA0 683 1F 0 0 0 0 0 0 RSSI1 3F800000 00000000 DBBA0 683 1F 0 0 0 0 D 19 RSSI2 3F800000 00000000 DBBA0 683 1F 0 0 0 0 0 0 RSSI3 3F800000 00000000 DBBA0 683 1F 0 0 0 0 0 0 RSSI4 3F800000 00000000 DBBA0 683 1F 0 0 0 0 0 RSSI5 3F800000 00000000 DBBA0 683 1F 0 0 0 0 0 0 not defined 0 1 7B2 1 F F 27 1F D59F8 0

The first two section represent the input ASCII command to the LiDAR and then the header of the received data packet. The header contains information like device status, encoder position, time of scans, channels etc. The next five sections starting with 'DIST' represent the five echoes and contains the respective distance values along with the following information.

DIST1 3F800000 00000000 DBBA0 683 1F 0 0 0 0 890B 8927

DIST1: Distance values for the first echo

3F800000: Scale factor (3F800000 = scale factor of 1)

00000000: Scale factor offset

DBBA0: Start angle of the scan

683: Angular resolution of the scan

1F: Number of measurement values for the first echo

0 0 0 0 890B 8927: Measurement values in HEX (units in mm)

The data format is similar for rest of the pulses.

2.2.1.2 Footprint of the LiDAR

The signal disperses as it further gets away from the source. This means that the diameter of the LiDAR beam increases as the distance to the object increases. Thus, the LiDAR beam occupies a conical space rather than a cylindrical one. The size of the beam at a certain distance is determined by the divergence angle of the beam. The energy of the beam is not uniformly distributed over its area and is approximated by a 2D Gaussian distribution. The total amount of energy in the beam remains constant even though the beam diameter changes at different distances. Hence, as the beam gets wider, the energy will also spread over a larger area leading to a lower signal to noise ratio. This might result in not detecting the target especially in bright illumination conditions. Figure 2.5 shows the method of calculating the footprint of the LiDAR.

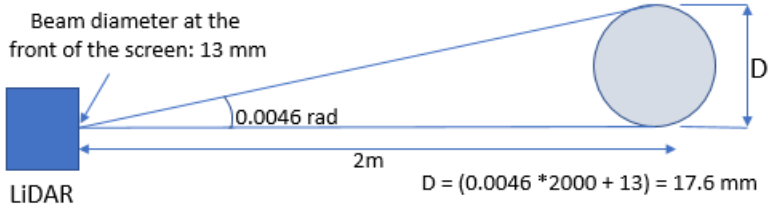

Figure 2.5. Calculation of the footprint of the LiDAR

2.2.1.3 Rotation Stage

A URS 150 BCC (Newport Corporation, Irvine, CA, USA) precision rotation stage was used to provide the rotational motion of plants. It has a maximum payload capacity of 300 N. It provides continuous 360°rotation with an angular resolution of 0.002°. The stage can rotate as fast as 80°/s. In our application, the rotational speed is maintained at 3°/s,

allowing 120 s for a complete rotation. Therefore, the point cloud generation time for each plant was two minutes. With the LiDAR scanning frequency at 25 Hz, the radial resolution of point clouds is 0.0021 radian. The stage connects to the computer via an RS-232 serial connection.

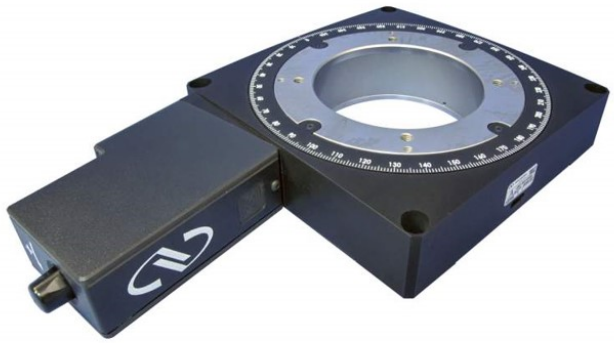

Figure 2.6. Roation stage used in the system (URS 150 BCC, Newport Inc.)

2.2.1.4 Synchronization between LiDAR values and the rotation stage angles

Figure 2.7 illustrates the logic behind the registration of the LiDAR measurements with the corresponding position in the rotation stage. As shown in figure, every slanted line represents one scan. The resultant motion of the rotation stage and the rotation mirror inside the LiDAR makes the scan line slanted. With an angular resolution of 1/6°, the number of data points in one scan is obtained as follows.

$$No.\ of\ data\ points\ in\ one\ scan\ = (stop\ angle - start\ angle) * 6 + 1 \qquad (2.1)$$

As we know the spacing between the points and the rotating speed of the internal mirror of the LiDAR, it is straightforward to calculate the relative time at which each point was detected for a single scan. With the speed of 25 Hz and the angular resolution of 1/6°, the

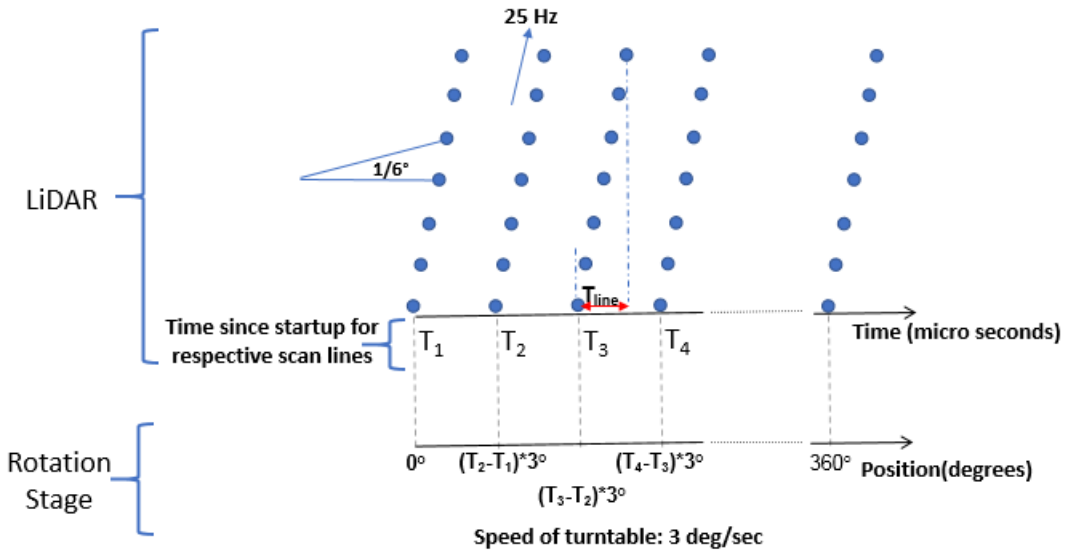

Figure 2.7. Schematic diagram for the synchronization of LiDAR values and the position of the rotation stage

time taken to obtain one data point is:

$$Time\ to\ scan\ a\ single\ data\ point = \frac{1}{6} * \frac{1}{25*360} * 10^6\ microseconds \qquad (2.2)$$

However, there is a small-time delay between the end of one scan and the start of subsequent scan and thus the start time of the next scan cannot be reliably calculated. Fortunately, each LiDAR data packet contains the time information that has elapsed after the device has powered on until the start of the individual scan. These time values (T1, T2, T3, etc.) can be taken as a reference time for the beginning of respective scans; and after that all the remaining data points for the scan can be calculated as shown in Equation 2.2. After the calculation of the time for individual data points, it is multiplied with the speed of the roation stage to get the angular position at which the data was captured. It is assumed that the speed of the rotation stage is constant with high degree of accuracy.

A LabVIEW (National Instruments) program was developed to control and synchronize the two devices (Figure 2.3(B)). The program allows the users to set the suitable scanning parameters and visualize the raw point cloud data in real time. The swath for the LiDAR

scanner is determined by the plant height, which in turn can be adjusted by entering the start angle and the stop angle of the laser beams in the program.

The URS150 BCC can be rotated in a discrete or continuous manner to acquire the entire or partial 360°degree point cloud. The continuous rotation was employed in our design, because it eliminates abrupt motions that cause plants to vibrate and lower the quality of the point clouds. Continuous rotation also improves the measurement throughput. The system also has some flexibility in determining the suitable height of the LiDAR platform and the distance to the rotation stage depending upon the size and shape of the plant.

During the scan, after one sweep of the laser beam in the vertical direction, the data packet received from LiDAR is parsed with the LabVIEW program and written to a spreadsheet file. The data string received is encoded in hexadecimal format, which contains information about device parameters (e.g., device number, device status, time since startup, etc.), scan parameters (e.g., resolution, frequency, start angle, stop angle, etc.), distance values and reflectance values. The measured distance R between the LiDAR and the target point is registered along with the beam angle and the rotation stage angle , using the scan frequency of the LiDAR, speed of the rotation stage and the scan starting time values given by the LiDAR as explained earlier.

2.2.1.5 Coordinate System

The vertical scanning plane of the LiDAR passing through the center of the rotation stage was considered the XZ plane with the center of the stage as the origin (Figure 2.8). The measurements obtained from the LiDAR were converted into XYZ Cartesian coordinates using the following equations.

$$X = (D - R\cos\theta) * \cos\phi \tag{2.3}$$

$$Y = (D - R\cos\theta) * \sin\phi \tag{2.4}$$

$$Z = h + R\sin\theta \tag{2.5}$$

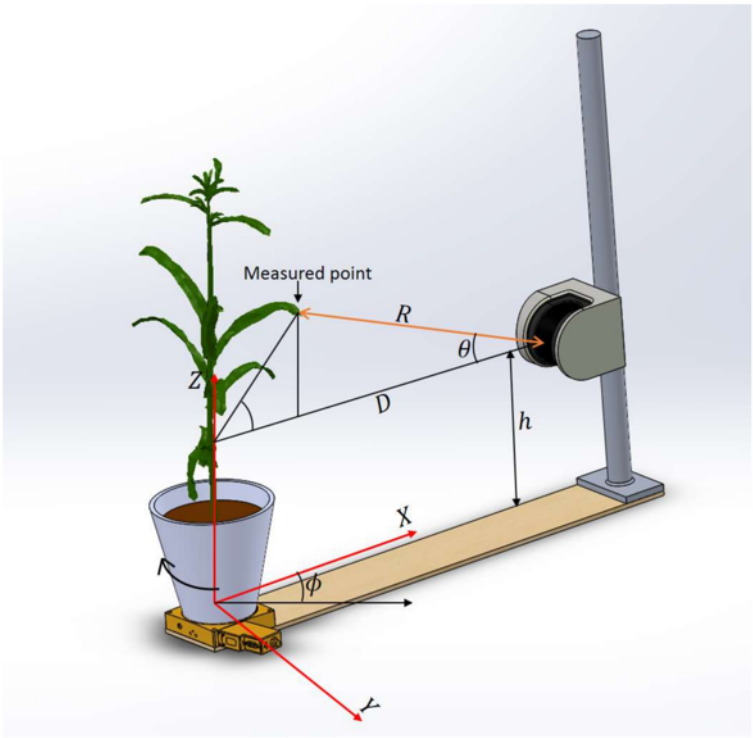

Figure 2.8. Coordinate system used to convert the range values from the LiDAR to Cartesian coordinates (Source: Thapa, Zhu, Walia, Yu, and Ge, 2018).

The fixed distance D between the LiDAR and the center of the rotation stage needs to be determined in advance for converting the LiDAR values into a reference frame. A simple measurement of the distance D with a measuring tape is not accurate and precise. Moreover, the manual measurements are error prone and it is challenging to find the reference point in the LiDAR which is taken as the basis for distance measurement. Hence, to increase the accuracy of the coordinate conversion, a thin vertical stick was placed in the center of the rotation stage and scanned with the LiDAR to find the horizontal distance between the

LiDAR and the z-axis of the coordinate system. Even though all the distance values should be same, they slightly vary and are almost normally distributed as shown in Figure 2.9.

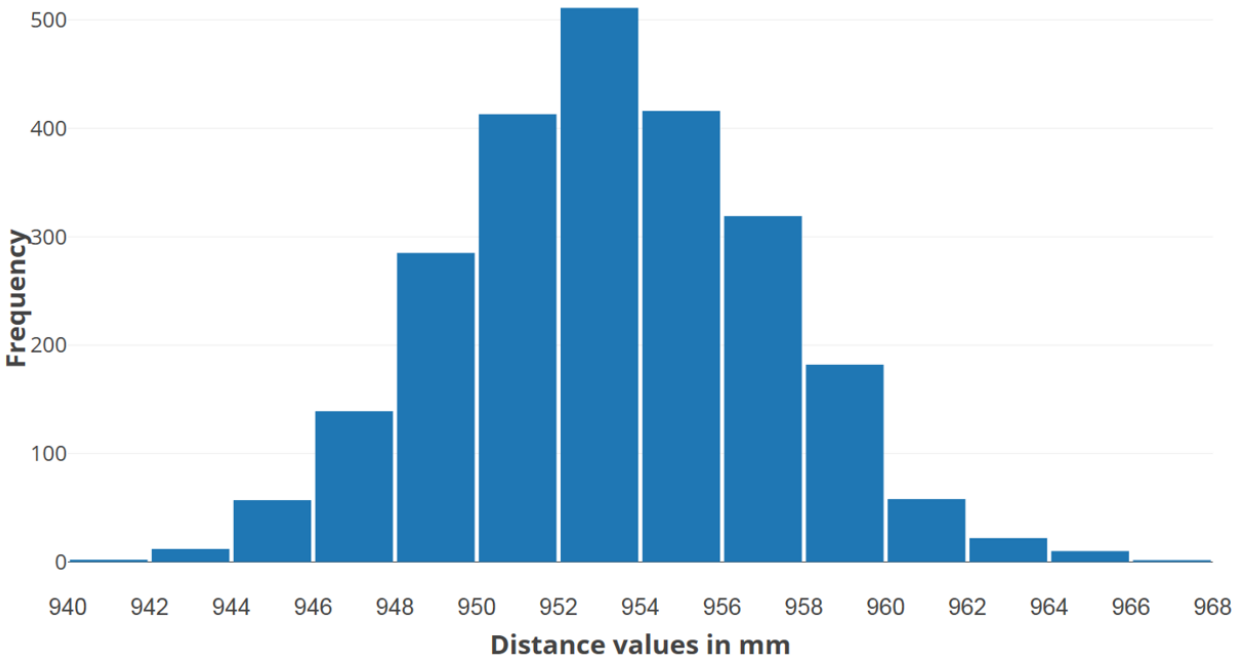

Figure 2.9. Distribution of LiDAR values

The mean value was taken as the distance D in the calculation for converting the LiDAR measurements in radial coordinate system to the Cartesian coordinate system.

2.2.2 POINT CLOUD PROCESSING ALGORITHM

The algorithm to process the raw plant point cloud data includes these steps: background removal, voxelization, clustering and segmentation, triangulation and surface fitting, and plant morphological trait extraction. Figure 2.10 shows an example of a sorghum plant from its raw point cloud to the final 3D model by going through these processing steps. The computing time to process a typical plant is 60 s.

Background removal: The point cloud data of plants generated by this new instrument contain part of the environment (e.g., the ceiling and walls of the room) and this part is called the background. The background is usually distinctive from the meaningful data of

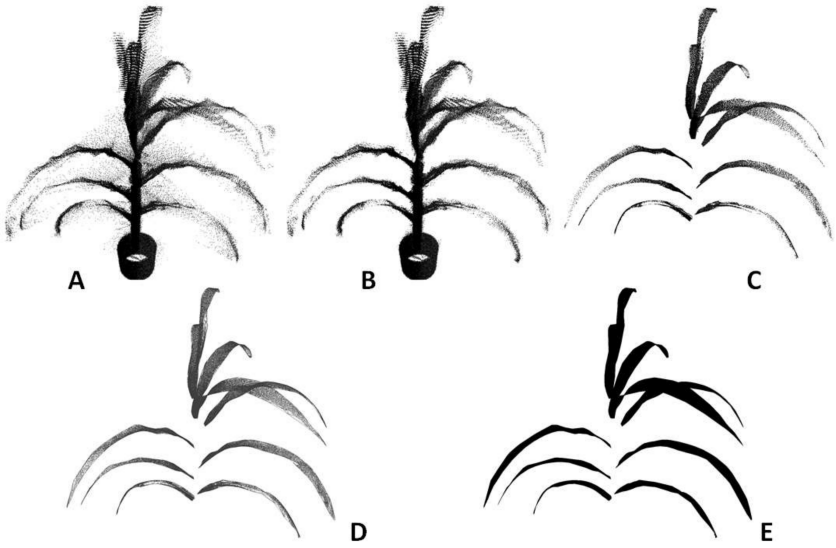

Figure 2.10. Example of 3D model of maize plant leaves after each step of point cloud processing: (A) raw point cloud of a maize plant derived by the instrument; (B) after voxelization and noise removal; (C) after clustering and segmentation; (D) after surface fitting and triangulation; and (E) a 3D rendering of the digital leaf surface model of the plant (Source: Thapa, Zhu, Walia, Yu, and Ge, 2018).

the plants in terms of the depth and is removed by limiting the XYZ range of the point cloud data.

Voxelization: Raw point cloud data are logged in a 2D matrix where every row corresponds to the 3D position (XYZ) of a point. The order of storing the positions is random and one point is not necessarily spatially close to its nearby points in the 2D matrix. This format is not optimal for data processing in later steps. To overcome this problem, voxelization was employed to transform the point cloud data into 3D matrix (Karabassi, Papaioannou, & Theoharis, 1999). The resultant 3D matrix maintains the locality of the point cloud data, as every point is spatially close to its nearby points. Voxelization also helps to remove the noise in the point cloud further, because it estimates the point density of each voxel. Noise commonly has lower point density and therefore can be removed by setting a suitable threshold (which is determined heuristically).

Clustering and segmentation: The pot and the stem were removed from the data by filtering the points within a suitable radius from the center. This step made the leaves to

be spatially separated from each other. K-means clustering was then used to segment the points that belonged to each leaf by feeding the k-value as the number of leaves in the plant (Arthur & Vassilvitskii, 2007).

Surface fitting and triangulation: Once the points belonging to a leaf were segmented, LOWESS (locally weighted scatterplot smoothing) was used to reconstruct the leaf surface (Cleveland, 1981). At each local region of the cluster, a quadratic polynomial function was fitted to a subset of data points using weighted least squares. The process was repeated for all the segmented leaves in a plant.

Although the surface can be well represented using some functions after surface fitting, it cannot be used directly to generate a 3D model. The surface needs to be discretized to a 3D triangular mesh before it can be visualized and processed further using computer graphics. The Delaunay triangulation algorithm (Fortune, 1992) was used to generate a triangular mesh based on a set of points such that no point is inside the circumference of any triangle in the mesh. A triangular mesh was generated in the XY-plane using the X and Y values of the original 3D points and the Z value corresponding to each vertex of the triangle was obtained through the polynomial function of the fitted surface. The triangular mesh was elevated into the 3D space using the Z values and a 3D triangular mesh for a leaf was completed. The reconstructed 3D mesh of a plant leaf is shown in Figure 2.11.

Plant morphological traits extraction: Four plant morphological traits were extracted from the leaf surface model as shown in Figure 2.11—area of individual leaf, total leaf area of the plant, leaf inclination angle (the angle at which a leaf emerges with respect to the stem), and leaf angular distribution of each plant. Individual leaf area was obtained by adding the area of all the triangular meshes that form the leaf surface (Figure 2.11). Similarly, total leaf area was obtained by adding the area of all individual leaves from a plant. Leaf angle was measured as the angle between the leaf blade and the horizontal surface at each leaf node. To obtain leaf angular distribution, first the orientation (surface normal) of each triangle was obtained and the fraction of this triangle area to the total plant

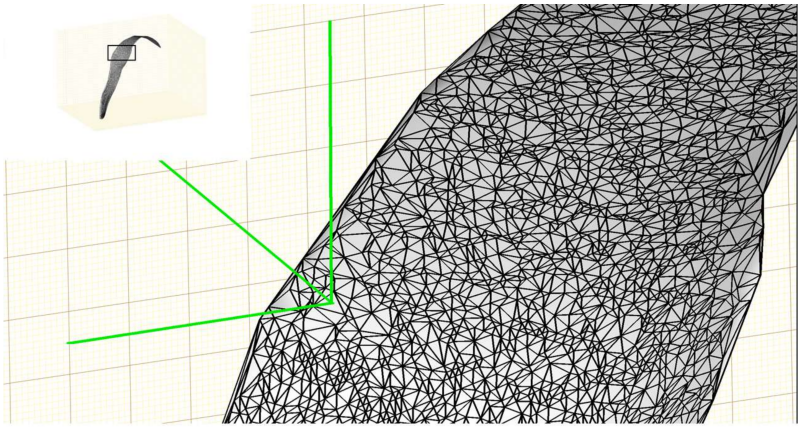

Figure 2.11. Example of triangulation of a fitted leaf surface in order to calculate leaf area, leaf inclination angle, and leaf angular distribution (Source: Thapa, Zhu, Walia, Yu, and Ge, 2018).

leaf area was calculated. The elevation angle in the surface normal vector was extracted (0°means horizontal leaf and 90°means vertical leaf) and the corresponding proportion was summarized into 10°bins. Finally, the histogram of area fractions versus the angle bins was plotted as leaf angular distribution.

2.2.3 EXPERIMENT TO VALIDATE THE INSTRUMENT

To validate the instrument for leaf area and leaf angle measurement, 20 plants (ten maize (B73) and ten sorghum (Tx430)) were grown in the LemnaTec phenotyping greenhouse at the University of Nebraska-Lincoln. Plants were grown under non-stress conditions. The validation experiment began after the plants were six weeks old. In each week, four plants (two maize and two sorghum) were randomly selected for data collection. Therefore, data collection was completed in five weeks, in which the plants spanned several vegetative stages (e.g., for maize, from V6 to V11, plant height roughly 1.6 m at V11). This procedure allowed the instrument to be validated on plants of varying sizes and canopy complexity.

The data collection steps were as follows. First, the selected plant was scanned with the new instrument to obtain its raw 3D point cloud. Second, an RGB image of the plant was taken. The purpose of the RGB image was to (1) allow a side-by-side comparison of

each plant and its point cloud and 3D model generated by the instrument; and (2) measure the angle between the plant's individual leaves with respect to its stem as the reference method of leaf inclination angle. After imaging, all leaves on the plant were cut and leaf area was measured by a leaf area meter (Model LI-3100C, LI-COR Biosciences, Lincoln, NE, USA).

The raw plant 3D point cloud was processed with the algorithms described in Section 2.2 to obtain the area of individual leaves and the whole plant, inclination angle of individual leaves, and leaf angular distribution of the whole plant. MATLAB (version 2016, MathWorks®, Natick, MA, USA) was used for point cloud processing. A correlation analysis was conducted to relate parameters derived from the 3D leaf surface model to those derived from the reference methods. Accuracy was assessed using R^2 (coefficient of determination) and mean absolute error (MAE).

2.3 RESULTS AND DISCUSSION

2.3.1 LEAF AREA

Figure 2.12 shows the 3D model of a maize and sorghum plant after point cloud processing. It demonstrates that the 3D models were similar to the actual plants with regard to the overall canopy structure. The maize plant had nine leaves, all of which were reconstructed in 3D. Similarly, the sorghum plant had eight leaves; and they were reconstructed successfully in 3D as well.

It can be seen from Figure 2.13 that 3D models give accurate, direct measurement of area of individual leaves. For maize, R^2 between model-derived leaf area and the reference measurement was 0.92 and MAE was 43.2 cm^2. Given the average maize leaf area of 463 cm^2 in this study, the MAE represents an error rate of 9.3% of the average maize leaf area. For sorghum, R^2 between the two sets of measurement was 0.94 and MAE was 16.0 cm^2. The average sorghum leaf area is 170 cm^2. Therefore, the MAE represents an error rate of 9.4% of the average.

Figure 2.12. Side-by-side comparison of the RGB image of a maize and a sorghum plant and their 3D models obtained by the new instrument. The segmented individual leaves are labeled (1 through 9 for maize, and 1 through 8 for sorghum) sequentially for easy comparison (Source: Thapa, Zhu, Walia, Yu, and Ge, 2018).

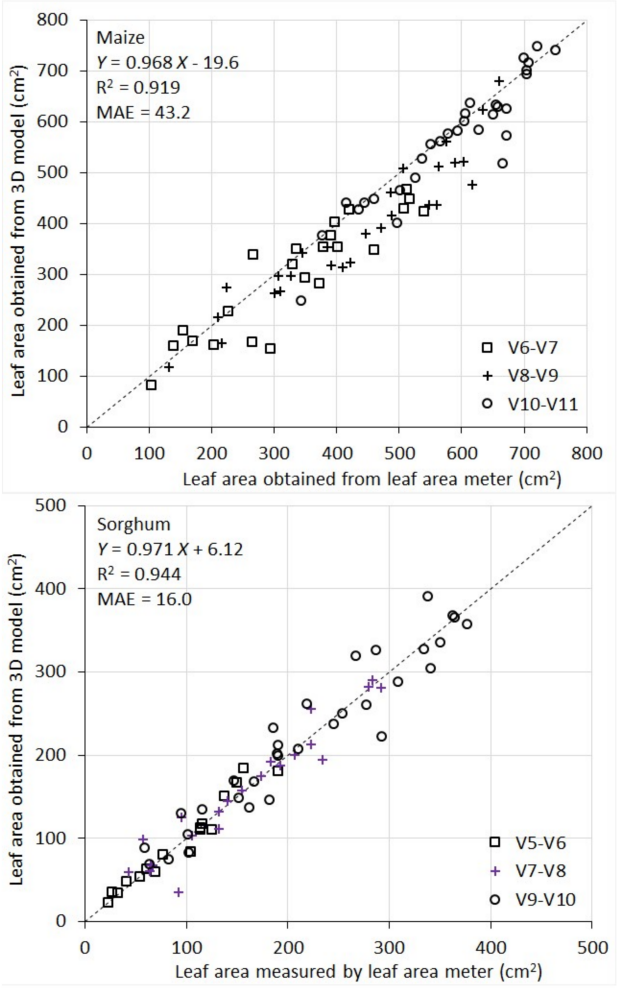

Figure 2.13. Scatterplot of individual leaf areas of 10 maize and 10 sorghum plants measured by the leaf area meter vs. obtained from 3D plant models. Different legends indicate different growth stages (Source: Thapa, Zhu, Walia, Yu, and Ge, 2018).

The performance of the instrument for leaf area measurement is also comparable across the developmental stages being evaluated (for maize V6 to V11, and for sorghum V5 to V10). This can be seen in Figure 2.13, where the scatters of the points for the different stages are consistent with each other.

For maize, there appears to be a systematic underestimation of individual leaf area by the 3D models compared to the area meter measurement. A closer examination of maize leaves (and their images) reveals that they have many local fine wrinkle structures particularly at leaf edges. The LiDAR point clouds are not quite effective to capture these local fine structures. Surface fitting (with 2^{nd} order polynomials) and triangulation tend to smooth them into a flat surface, which leads to a systematic underestimate of the leaf area. On the contrary, sorghum leaves are smoother and therefore better represented by low-order polynomials in surface fitting and triangulation, which leads to lower systematic errors in leaf area modeling.

In addition to the systematic underestimate of leaf area in maize plants, there are also random errors in the leaf area measurement for both species by the instrument (some overestimate some underestimate). The random error components are attributed to three sources. Firstly, although the rotational stage largely addresses the occlusion problem, some occlusion still occurs for a subset of plants, in particular those with more complex structure. Partially occluded leaves cannot be reconstructed accurately (hence underestimated). Secondly, the LiDAR has an intrinsic accuracy limitation in distance ranging. This random error makes a smooth leaf surface appear rough during surface fitting and triangulation, thus leading to an overestimate of the area. Thirdly, the stem of the plants are thicker at the bottom and thinner at the top. Since we apply a constant distance filter to remove the stem points in point cloud processing, it causes slight area underestimate for top leaves and overestimate for bottom leaves.

In many applications, it is the total leaf area rather than areas of individual leaves that needs to be measured or modeled. When individual leaf area was aggregated to total leaf

area of a plant, the accuracy of the 3D models was increased (Figure 2.14). For maize, R^2 was 0.95, and for sorghum R^2 was 0.99. Aggregation from individual leaves to the whole plants removed random errors (overestimation vs. underestimation) and increased correlations. A closer examination indicated that the 10 maize plants were clustered into two groups in terms of total leaf area. This clearly inflated the R^2 value as the maize plants exhibited larger scatter around the regression line compared to sorghum. Nevertheless, the high R^2 values for both species suggest the new sensor can be a powerful tool to measure this important plant trait with higher accuracy.

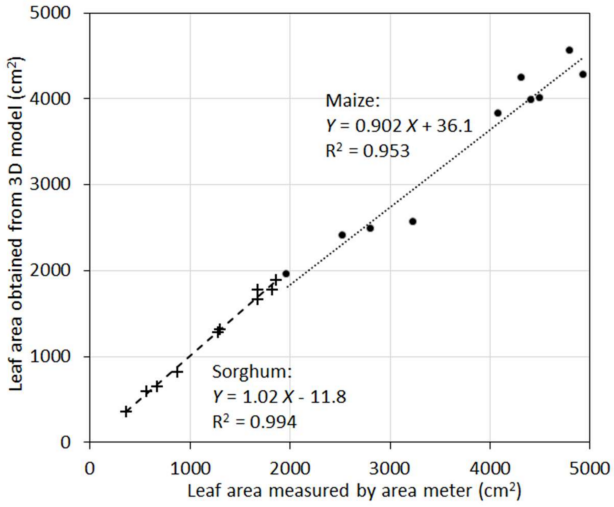

Figure 2.14. Scatterplot of total leaf areas of the 10 maize plants (circles) and 10 sorghum plants (crosses) measured by the leaf area meter vs. obtained from 3D plant models (Source: Thapa, Zhu, Walia, Yu, and Ge, 2018).

In plant phenotyping, RGB images from multiple side views and top view were commonly used to estimate plant leaf area (Ge et al., 2016; Klukas et al., 2014). Because images only capture projected leaf area on 2D, empirical equations were developed to relate multi-view 2D projected leaf areas to the actual leaf area in 3D. The problem with this approach is that the empirical equations are dependent on plant species, their developmental stage, and even treatment effects. This represents a limitation of using RGB imaging to measure leaf area because, for each application, some plants have to be destructively sampled to build the empirical equation, which would lower the throughput

of analysis. On the contrary, the platform we have developed directly measures plant leaf area in 3D. It eliminates the need of destructive sampling and will greatly improve the throughput of measurements.

2.3.2 LEAF ANGLE

The correlation between leaf inclination angles measured from 2D images and those obtained from the 3D model was given in Figure 2.15. For maize plants, the two sets agree with each other well (R^2 = 0.904) and the difference appears mainly to be random errors. Sorghum plants show a lower correlation (R^2 = 0.723). There is an overall overestimation for leaf angle measured from the 2D images. This is because, for maize, there exists a plane in 3D where all the plant leaves are aligned. Since RGB images are taken in this plane, the images preserve the leaf inclination angle well. Whereas for sorghum plants, their leaves are distributed in all directions. Measurements of leaf inclination angle from their images lead to an overestimation for the leaves that grow into or out from the imaging plane. To make a better comparison, we selected the sorghum leaves that are aligned in the imaging plane by examining both the plant images and the 3D surface models. When only this subset of leaves is considered (black circles in the sorghum plot of Figure 2.15), the R^2 value is 0.81 and the systematic underestimation is greatly reduced.

The 3D plant leaf models created by our instrument therefore overcome the limitation for leaf inclination angle retrieval from 2D images, and further enables the calculation of leaf angular distribution, which is even more challenging with 2D imaging.

2.3.3 LEAF ANGULAR DISTRIBUTION

The leaf angular distributions of the maize and sorghum plants in this experiment are given in Figure 2.16. For maize, the proportion of leaf area increased quickly from lower angles (horizontal leaf) to higher angles and peaked at 75°. For sorghum, the distribution of leaf angle increased more gradually from lower to higher angles. Whereas the maize plants

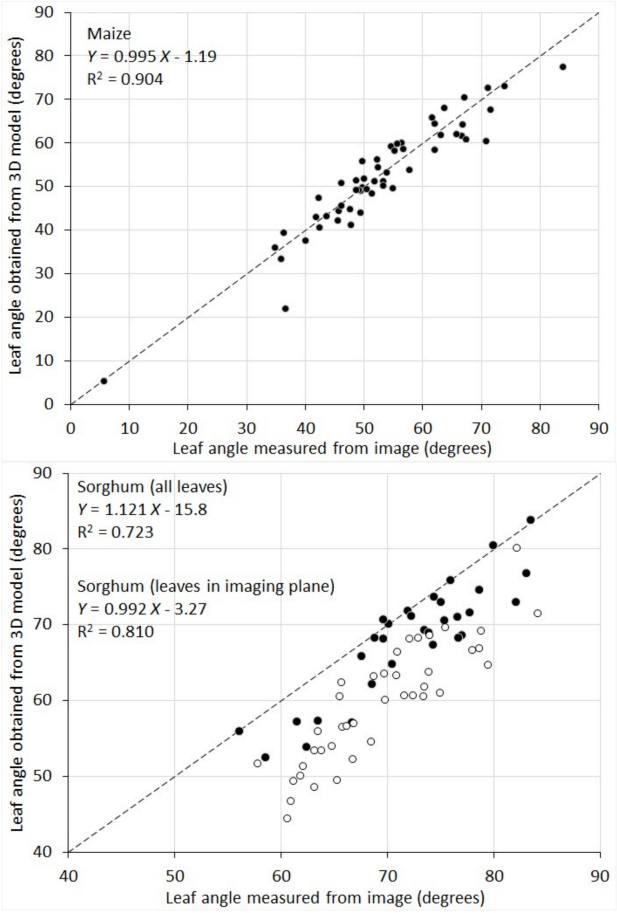

Figure 2.15. Scatterplot of individual leaf angle of ten maize and ten sorghum plants measured from their RGB images vs. obtained from 3D plant models. For sorghum, solid dots represent the leaves aligned in the imaging plane and hollow dots represent the leaves not in the imaging plane (Source: Thapa, Zhu, Walia, Yu, and Ge, 2018).

have a single peak at 75°, the leaf angular distribution of the sorghum plants has a plateau between 45°and 75°.

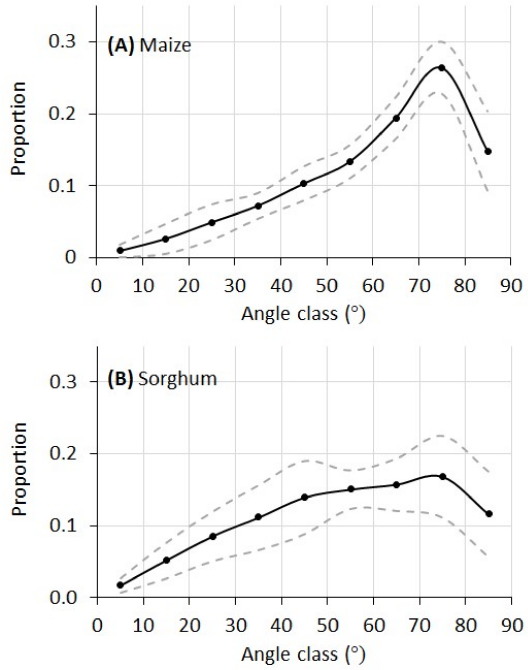

Figure 2.16. Leaf angular distribution of the ten maize plants and ten sorghum plants derived from their 3D leaf surface model. Solid line is the average proportion and the dashed lines are one standard deviation from the average (Source: Thapa, Zhu, Walia, Yu, and Ge, 2018).

As stated earlier, manual direct measurement of leaf angular distribution (LAD) needs alignment of an inclinometer at each and every leaf segment of a plant. For plants like maize and sorghum with large and curvy leaves, this could be very tedious if not impossible. Therefore, a validation of the LAD curves in Figure 2.16 with manual measurement was not conducted. However, limited published data on LAD provide validation on our measurements. For example, a maize canopy LAD reported in Ross (Ross, 1981) shared much similarity compared to our measurement in Figure 2.16A, with a rapid increase from low to high angles and a peak at 75°. A sorghum canopy LAD reported in Goel and Strebel (Goel and Strebel, 1984) also matched our measurement in Figure 2.16B, with a gradual increase of leaf proportion from low to high angles with the largest proportion between 45 and 75°. Theoretically, plant canopy LADs can be modeled

by a general ellipsoidal function with Campbell's x parameter (G. S. Campbell and Norman, 2012; Jones, Coops, and Sharma, 2010). It can be seen that both maize and sorghum plants in this study exhibited typical erectophile distribution (meaning higher proportion of vertical leaf segments than horizontal leaf segments), which can also be verified from the RGB images of these plants.

The leaf angle of both maize and sorghum plants was studied (Mccormick et al., 2016; Strable et al., 2017) to elucidate its genetic control. A very important aspect of leaf angle is that planting density can be higher for genotypes exhibiting more erect angular distribution. The new instrument can potentially be used as a nondestructive and rapid tool for selecting genotypes with desirable leaf angle and angular distribution for crop improvements or evaluating large mapping or mutant populations to understand the genetic control of these leaf-angle related phenotypes (Truong, McCormick, Rooney, and Mullet, 2015).

2.3.4 PLANT BIOMASS

3D modelling of the plant also provides information on numerous additional parameters like plant height, leaf length, leaf width, biomass, volume etc. To observe the relationship between the total surface area and the biomass, fresh shoot weight of the individual plants was plotted against the total leaf area of respective plants. The prediction models for both maize and sorghum plants show a high correlation ($R^2 \geq 0.94$) between the total leaf area and the fresh weight which implies that total leaf area can be used to estimate the biomass of the plants (Figure 2.17).

As surface area of a part is correlated with its volume, modelling techniques might also be used to predict the volume of the plant parts. Volume measurements are required to determine the shoot-root ratio of the seedlings which can be used in growth studies. One of the obvious ways to measure the volume of plant parts is to dip them in a water vessel and obtain the volume of displaced water. However, such primitive method is tedious and

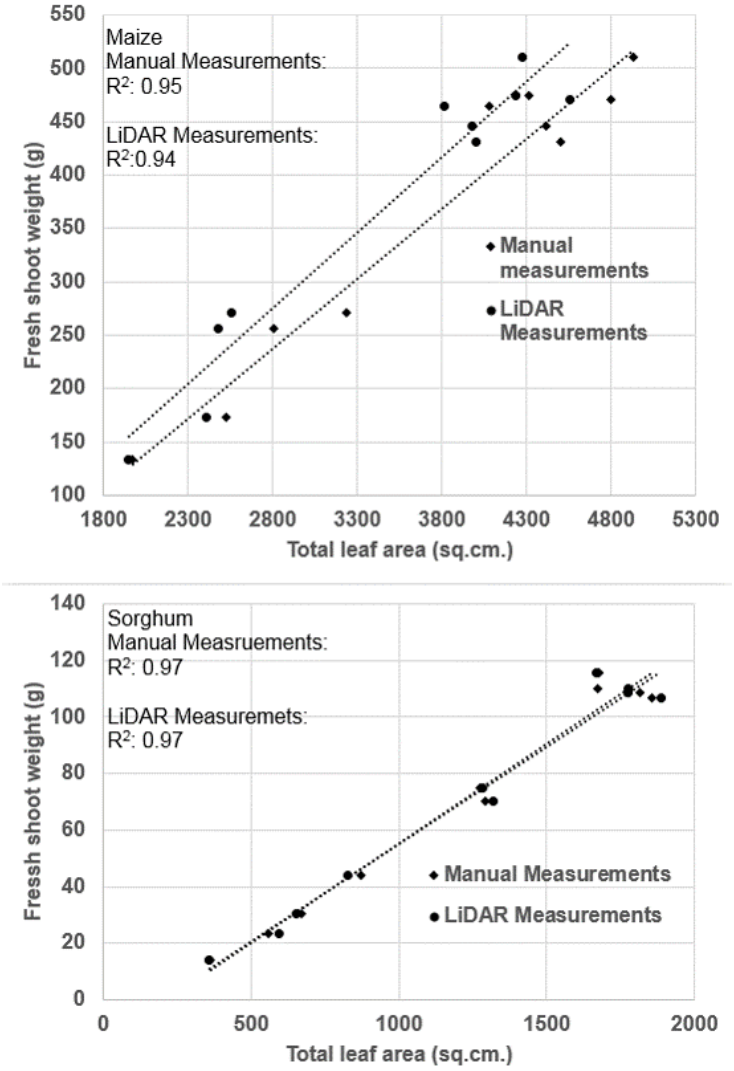

Figure 2.17. Scatterplots showing the relationship between biomass of the plants and total leaf area of the plants. Total leaf area of the plants is obtained from manual measurements as well as from the LiDAR measurements.

requires destructive sampling of the plant. Hence, 3D models of the plants may come handy in such purposes as volume of a plant might be inferred from its 3D model.

Although the validation results demonstrated the potential of the new instrument, few limitations are noted and should be worked on to improve the instrument. First, the maize and sorghum used to test the new instrument have a relatively simple plant structure and large leaves, compared to plants like soybean or cotton. The denser leaf structure of these species makes it more challenging to capture the complete point cloud of the canopy (due to occlusion), and smaller leaves further reduce the efficiency for surface reconstruction. Secondly, a few system parameters are provided manually, including starting and stop angles and LiDAR height for point cloud generation, as well as the threshold for point cloud noise removal and the leaf number for k-means clustering in point cloud processing. This is undesirable in practical settings. Lastly, if the stem of the plant is not upright, removing the stem part from the raw point clouds will be challenging.

Apart from these, LiDAR has some inherent size limitation in detecting the object. The laser beam must be totally incident on the plant surface in order to be reliably detected. If a beam is partially incident, the energy reflected is lower and may not be properly detected by the receiver. An object is reliably fully seen when it is at least as large as the beam diameter plus the point spacing between the beams as shown in Figure 2.18. The point spacing is determined by the angular resolution of the LiDAR and the beam diameter (LiDAR footprint) is determined by the divergence angle of the beam as explained earlier. Hence, young and slender leaves as well as edges, tips and petioles of the leaves may not be detected by the LiDAR.

Moreover, the problem of occlusion is not totally eliminated even in case of the LiDAR scan. As shown in Figure 2.19, some points are missing on the surface of the leaves as either the laser pulse fails to strike the surface or is mostly scattered away and is not being detected by the sensor. This happens because of the position of the LiDAR in combination with shape (rolled, bent, twisted etc.) of the leaf, orientation of the leaf, and the canopy

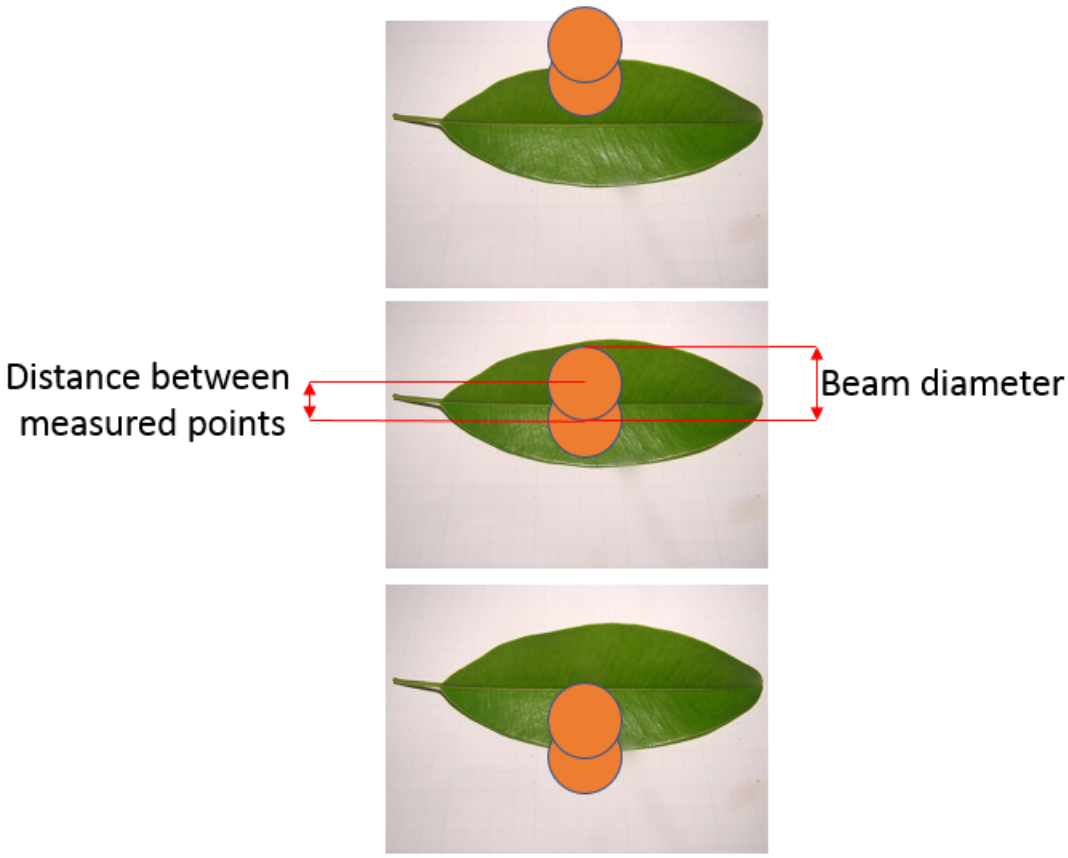

Figure 2.18. Minimum object size for detection by the laser pulse.

architecture (how bushy it is). The loss of information in such a way may contribute to the result being less accurate for such leaves.This is not much of a problem unless the missing points are from the edge causing the loss of the boundary. One potential solution of further reducing this problem of occlusion may be scanning the target from multiple views as in case of 2D imaging and then combining those scans to achieve a better point cloud. However, this comes with a significantly larger cost of time and computing power which should also be considered in practical applications. Also, in future, multiple echoes from the LiDAR can be recorded and then tested to see if it improves the quality of point cloud by mitigating the occlusion.

We would also like to improve the instrument in the following two aspects. First, we will incorporate lasers of multiple wavelengths into the instrument, which would allow for the measurement of chemical or physiological traits of plants. Second, we will seek to integrate the instrument with an automated conveyor belt such as LemnaTec Scanalyzer 3D system (Golzarian et al., 2011; Pandey, Ge, Stoerger, and Schnable, 2017) to maximize its capacity for plant morphological trait measurement.

2.4 CONCLUSION

This paper reported the development and validation test of a new LiDAR-based instrument for high-throughput, nondestructive measurement of plant morphological traits for single maize and sorghum plants. The following conclusions are drawn from this study.

- The instrument effectively generates a 3D point cloud of plants at a 360° view, with a measurement speed of 2 min per plant.
- The point cloud processing pipeline reduces point clouds to digital leaf surface model, with a processing speed of 60 s.
- Both the leaf area and the leaf inclination angle obtained from the 3D leaf surface model are highly correlated with those measured by the validation methods (R^2 from 0.72 to 0.99).

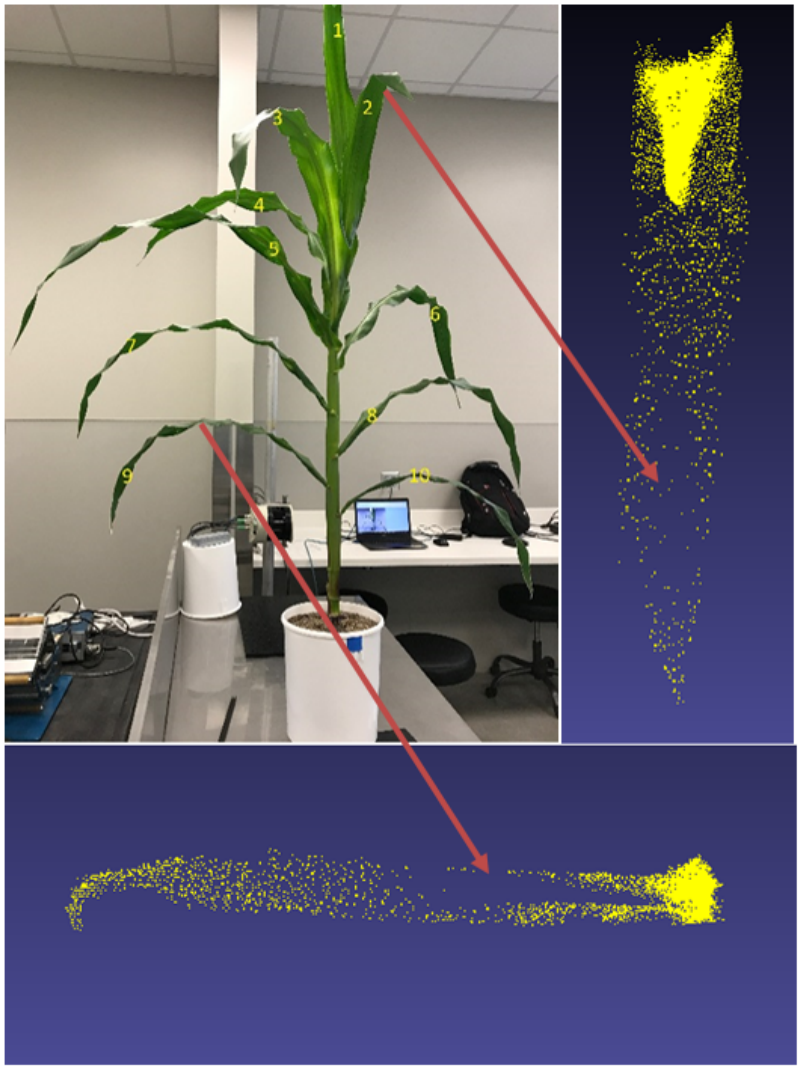

Figure 2.19. Image showing the structure of the two maize leaves in an RGB image and their corresponding point clouds. Some portion of the leaves are poorly detected by the LiDAR due to curved geometry of leaves.

- Generation of leaf angular distribution from 3D leaf surface model is demonstrated.
- Plant biomass can also be derived from the 3D model of the plant.
- With some future improvement, the instrument can potentially fill the current technological gap to enable direct, rapid, and nondestructive measurements of plant leaf area and leaf angular distribution.

CHAPTER 3

GENERATION OF SPECTRAL 3D POINT CLOUD USING STRUCTURE FROM MOTION TO MEASURE CHEMICAL PROPERTIES OF MAIZE

3.1 BACKGROUND

Structure from motion (SFM) is a photogrammetric technique of reconstructing a 3D model based on a sequence of images taken from multiple viewpoints. This technique computes the camera poses for each of the images and detects the relative motion of the cameras.

The first step in 3D reconstruction involves finding the key points in the images. After extracting the key features in the images, they are matched between multiple images. Using this information, fundamental matrix and then essential matrix are computed. Finally, projection matrices are computed which gives the 3D points for the object.

In 2012, Paproki, Sirault, Berry, Furbank, and Fripp (2012) took high resolution multiview images (10 megapixels) of cotton plants placed in a rotating tray and then used a commercial 3D digitization software called 3DSOM to create the plant models. Similarly, this method of 3D reconstruction from multiple 2D images has been applied by several other people for creating 3D plant geometry (Gibbs et al., 2015; Liu, Acosta-Gamboa, Huang, and Lorence, 2017; Pound, French, Murchie, and Pridmore, 2014; Santos and De Oliveira, 2012).

3.1.1 SPECTROSCOPIC MEASUREMENT OF CHEMICAL PROPERTIES

The interaction of plants with electromagnetic spectrum is unique. A typical vegetation spectrum exhibits a non-uniform distribution of reflectance values which forms the basis for chemical measurements. A green healthy plant absorbs most of blue, green and red light,

strongly reflects in the near infrared region, and highly absorbs the shortwave infrared in some wavelengths due to presence of water in leaf. The variation in the spectrum is caused by factors like cellular structure, pigments, water content, and organic compounds which exhibit different absorption features. Monitoring these spectral differences and studying their relationship to the physiological properties of plants allows the inference of plant health status.

Different remote sensing techniques have been applied to measure reflectance data for predicting the physiological or biochemical properties. Hyperspectral imaging is popular technique that captures the images in the narrow (usually $<$ 10 nm), contiguous spectral bands, with a spectral range from about 300 nm to 2500 nm. The spectral signature of the plant obtained for each pixel at different bands can be combined and compared to reveal vegetation characteristics. These are also called Vegetation Indices (VIs). For example, Normalized Difference Vegetation Index (NDVI) is an index calculated from reflectance values at red and near-infrared bands. In agriculture, NDVI is used in a lot of applications such as in predicting biomass of crops (Freeman et al., 2007) , nitrogen content (Tremblay, Wang, Ma, Belec, and Vigneault, 2009), drought (W. T. Liu and Negrón Juárez, 2001)(Karnieli et al., 2010), yield (Ma, Morrison, and Dwyer, 1996), soil erosion (Yengoh, Dent, Olsson, Tengberg, and Tucker, 2016) and many more. Hyperspectral image data have been used with statistical modelling techniques such as Partial Least Square Regression (PLSR) for non-destructive measurement of leaf chemical properties such as nitrogen, phosphorous and chlorophyll (Pandey et al., 2017).

Though structural properties and biochemical properties of plants have been well determined separately, there is lack of research work assessing these properties simultaneously and that too in 3D. Measurement of these properties with a single instrument will greatly benefit plant phenotyping by not only providing high quality morphological and physiological data but also reducing the time and cost incurred by multiple separate measurements.

3.1.2 SPECTRAL 3D SENSING

There have been a few efforts in combining the spatial and spectral intensity information together by combining laser scanned point clouds with the hyperspectral images (Jones et al., 2010; Puttonen, Jaakkola, Litkey, and Hyyppä, 2011; Thomas et al., 2009). Strothmann, Ruckelshausen, and Hertzberg (2014) used four different types of lasers along with a monochrome camera to create a 3D point cloud with spectral information. Wei et al. (2012) developed a multiwavelength LiDAR and demonstrated its performance in detecting nitrogen stress in rice leaves. A very novel hyperspectral LiDAR was developed by Hakala, Suomalainen, Kaasalainen, and Chen (2012) using supercontinuum lasers with a spectral range of 470-990 nm. They demonstrated the functionality of this instrument by generating a hyperspectral point cloud of Norwegian spruce and calculating different vegetation indices from the 3D spectral data.

3.1.3 MODELLING TECHNIQUES

Four different modelling techniques were applied in this study to estimate the nutrient content and water content of the plants as a function of the reflected color values at seven channels. The four methods employed are Partial Least Squares Regression (PLS), Artificial Neural Network (ANN), Random Forest (RF) and Support Vector Regression (SVR).

Partial Least Squares Regression (PLS) is a linear modelling technique applied when there are a large number of independent variables exhibiting a high degree of multi-collinearity. PLS reduces the number of dimensions as in principal component analysis and creates new variables, also called ‘latent variables’ by considering both the independent variables and the response variables. The tuning parameter used to optimize this kind of model is the number of latent variables (n_{LV}) used in the regression.

Artificial Neural Networks (ANN) is a non-linear modelling technique inspired by the structure of a biological neuron and comprises of a multiple layers of nodes(neurons).

These neurons receive information from neurons in the previous layer and combines them in some way (usually multiply with a weight and add a bias), and then perform a non-linear operation to give a final result. During the training process, the error from the model is minimized by backpropagation through adjusting weights and biases of the nodes. Number of hidden layers, number of nodes in each layer and learning rates are the common parameters of the ANN model that are used for model tuning.

Random forest is an additive modelling technique that operates by constructing a number of decision trees during training and then makes predictions by averaging the results from the sequence of those individual trees. While creating a decision tree, only a subset of randomly selected features is taken into consideration for splitting a node. RF is popular due to its resistance to noise, capability to function even when there are higher number of predictor variables than the number of observations and, less overfitting. The number of trees to construct and the number of variables randomly sampled as candidates at each split (m_{try}) are the two main tuning parameters in RF.

Support Vector Regression (SVR) fits a regression function with at most ε deviation from the target by mapping the inputs into higher dimensional feature space through a kernel function. The main tuning parameter is called 'C' which penalizes the model for the violations of the permissible error boundary defined by parameter ε .

3.2 MATERIALS AND METHODS

3.2.1 DATA ACQUISITION

Structure from motion technique is used to create 3D point clouds at seven different spectral bands in which every point has value for the color information at that band. The concept is similar to hyperspectral imaging, however, unlike hyperspectral imaging, this process involves only a few numbers of spectral bands.

A scientific purpose CMOS camera (DCC3240N, Thorlabs) was used to take pictures of the plants. It is a monochrome camera with varying sensitivity to light between wavelengths

of 400 nm to 1100 nm. The properties of this camera are shown in Table 3.1 and the sensitivity graph of the sensor is shown in Figure 3.1.

Table 3.1. Specifications of the camera used to acquire images to construct the 3D point cloud

Sensor Type	CMOS
Shutter system	Electronic global shutter
Resolution	1250 x 1024 pixels (1.3 megapixels)
Aspect ratio	5:4
Bit depth	8 bits
Pixel size	5.30 sq. micrometer
Frame rate (free run mode)	60 fps
Exposure (free run mode)	0.009 – 2000 ms

The camera is highly sensitive to light in the visible range and the sensitivity decreases towards the near infrared region. Hence, the spectral data captured needs to be corrected for this difference in camera sensitivity to light at different wavelengths.

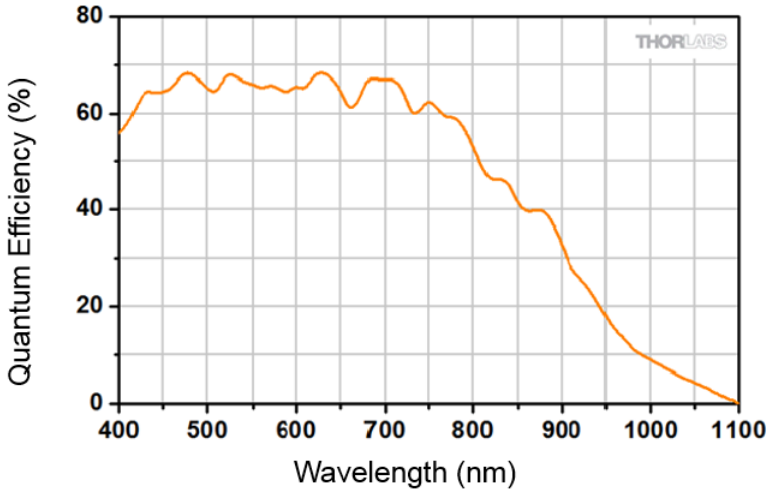

Figure 3.1. Quantum Efficiency (or Sensitivity) of the camera as a function of wavelength from 400 to 1100 nm (Source: Thorlabs).

Seven different narrow bandpass optical filters were used along with the lens of the camera to capture the images at specific bands of interest. The filter wavelengths used, and

their properties are listed in Table 3.2.

Table 3.2. Properties of the seven narrow band-pass filters used to acquire images at the selected spectral bands

S.N.	Center Wavelength (nm)	FWHM (nm)	Peak Transmission (%)	Blocking($<$ 0.01%) (nm)
1	530 ± 2	10 ± 2	50	200-3000
2	570 ± 2	10 ± 2	50	200-3000
3	660 ± 2	10 ± 2	50	200-3000
4	680 ± 2	10 ± 2	50	200-3000
5	720 ± 2	10 ± 2	50	200-3000
6	770 ± 2	10 ± 2	50	200-3000
7	970 ± 2	10 ± 2	50	200-3000

20 maize plants were grown in greenhouse for the experiment and were not subjected to any form of treatment. After 5 weeks from plantation, the plants had 6-8 leaves. The images of the plants were taken in a closed room illuminated by two halogen lamps, each of 1000-watt capacity. Around 50 images per plant were taken for each spectral band by moving around the plant with the camera placed on a dolly. A white board was also imaged at each band to obtain the reference light intensity value. After images were captured for one band, the filter had to be replaced and then the focus of the lens adjusted slightly as the focal length of the light depends on the wavelength. Exposure time of the camera was also adjusted because using the same exposure time for each bands would decrease the image quality as plants reflect different portion of energy at different wavelengths. The exposure time at near infrared bands is lower than that at visible bands as using the same exposure as used in visible bands would saturate the pixel values for the near infrared bands. After the plants were imaged, fresh weight of each plant was recorded. Finally, the plants were dried in an oven to constant weight, and the dry weight was recorded to calculate the water content of the plant samples.

3.2.2 DATA PROCESSING

Point clouds for all of plants at each of seven bands were generated by using VisualSFM, which is an interface for the structure from motion algorithm developed by Wu (2018). The point cloud generated has a 4-dimensional data structure, where the first three dimensions are the three spatial coordinates (x, y and z) and the fourth dimension is the spectral information at the corresponding wavelength. SFM algorithm extracts the color value for the 3D points from the image pixels.

After generating the point clouds, the inherent noise (mostly background including plant pot) lying in the point cloud was manually filtered using Meshlab software (Cignoni et al., 2008). The color values of each point cloud were extracted and then averaged over the whole plant to obtain a mean value to represent that plant. The mean color value was corrected for the exposure time and the camera sensitivity at the respective wavelengths. For the radiometric correction, a reference color intensity value was calculated by averaging the pixel values of the image of the white board taken at each band keeping the exposure time constant. Finally, the normalized color value was obtained for the seven channels for each of 20 plants. Also, it is noted that there was no any correction for the filter transmission because all the filters had similar transmission. This would not affect the results in the statistical modelling later on. The overall formula used for the correction of the spectral value is given in Equation 3.1.

$$corrected\ color\ value = \frac{mean\ color\ value}{exposure\ time \times camera\ sensitivity \times mean\ color\ value\ white\ panel} \tag{3.1}$$

The corrected color values at seven spectral channels were considered as the predictor variables used in the four different modelling techniques. The parameter n_{LV} was changed from 1 to 6 for optimizing the RMSE (Root Mean Square Error) during CV (Cross Validation) of PLS model. For ANN, different combinations of a single hidden layer containing 1 to 7 neurons and three different decay rates (0.01, 0.1 and 0.3) were used to

find the minimum RMSE during cross validation. For RF, the number of the variables available for splitting the tree (m_{try}) at each split was varied from 1 to 7 to find the minimum RMSE during cross validation.

The method of leave one out cross validation was used to find the optimum tuning parameters for all the four techniques as the number of samples were very limited for splitting them into a separate training and validation set. The performance of the four different models were compared by calculating R^2, RMSE (Root Mean Squared Error) and RPD (Ratio of Performance to Deviation).

3.3 RESULTS AND DISCUSSION

3.3.1 POINT CLOUDS AND THEIR SPECTRA

Figure 3.2 shows the point clouds obtained for the seven different bands for a plant after correcting for the exposure time and the camera sensitivity. Visually, we can see that the color becomes lighter as we move from 530 nm toward 970 nm, which is in accordance with the higher reflection of the NIR wavelengths by the plants.

Figure 3.3 shows the spectral curves that are obtained by averaging the color values at each band and then interpolated to make a smooth curve. The curves look similar to a typical green vegetation spectrum with lower reflection of the light energy in the visible bands followed by higher reflection in the near infrared bands. Since the spectral sampling of our image data is low, we do not see the peak in the visible range near 550 nm.

3.3.2 PREDICTION FOR WATER CONTENT (WC) AND NUTRIENT CONTENT (N, P, K)

Table 3.3 summarizes the results of modeling spectral data by four different approaches. Among them, RF performed consistently better for predicting WC, N, P and K.

Figure 3.4 shows the prediction for the four response variables – WC, N, P and K using the RF technique. Although these prediction models may not be robust and

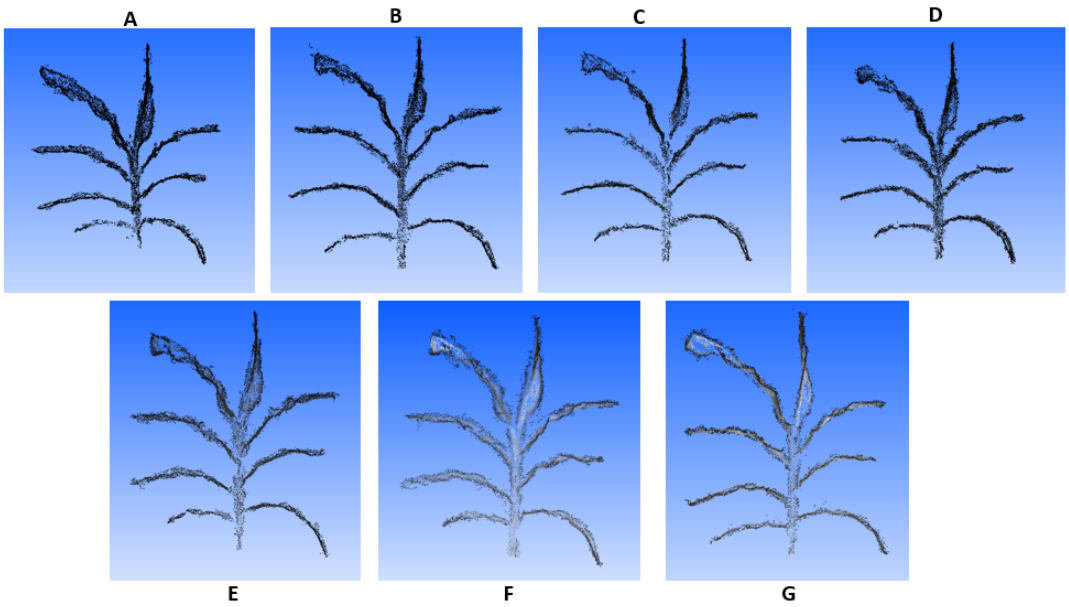

Figure 3.2. Visualization of the point cloud normalized for exposure time and camera sensitivity. Each point cloud contains the spectral information at following bands: (A) 530 nm (B) 570 nm (C) 660 nm (D) 680 nm (E) 720 nm (F) 770 nm (G) 970 nm .

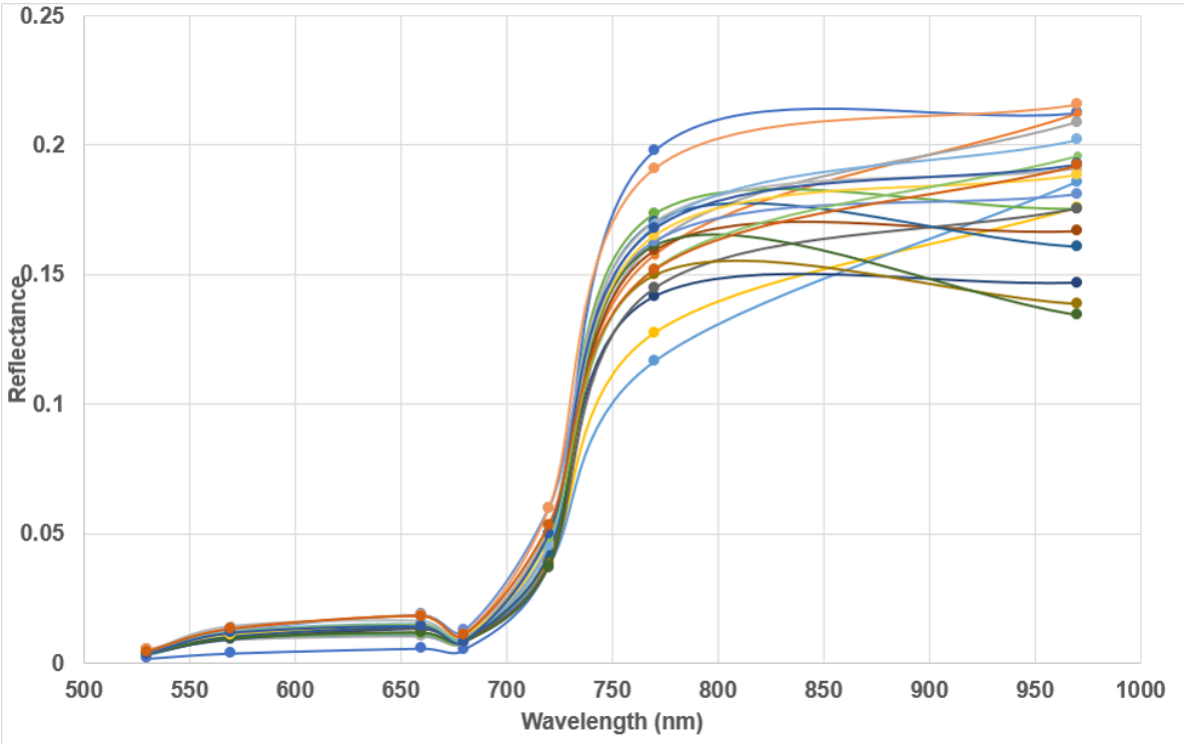

Figure 3.3. Spectral signature of the maize plants calculated from 7 different bands. The different colors of the spectra represent different plants.

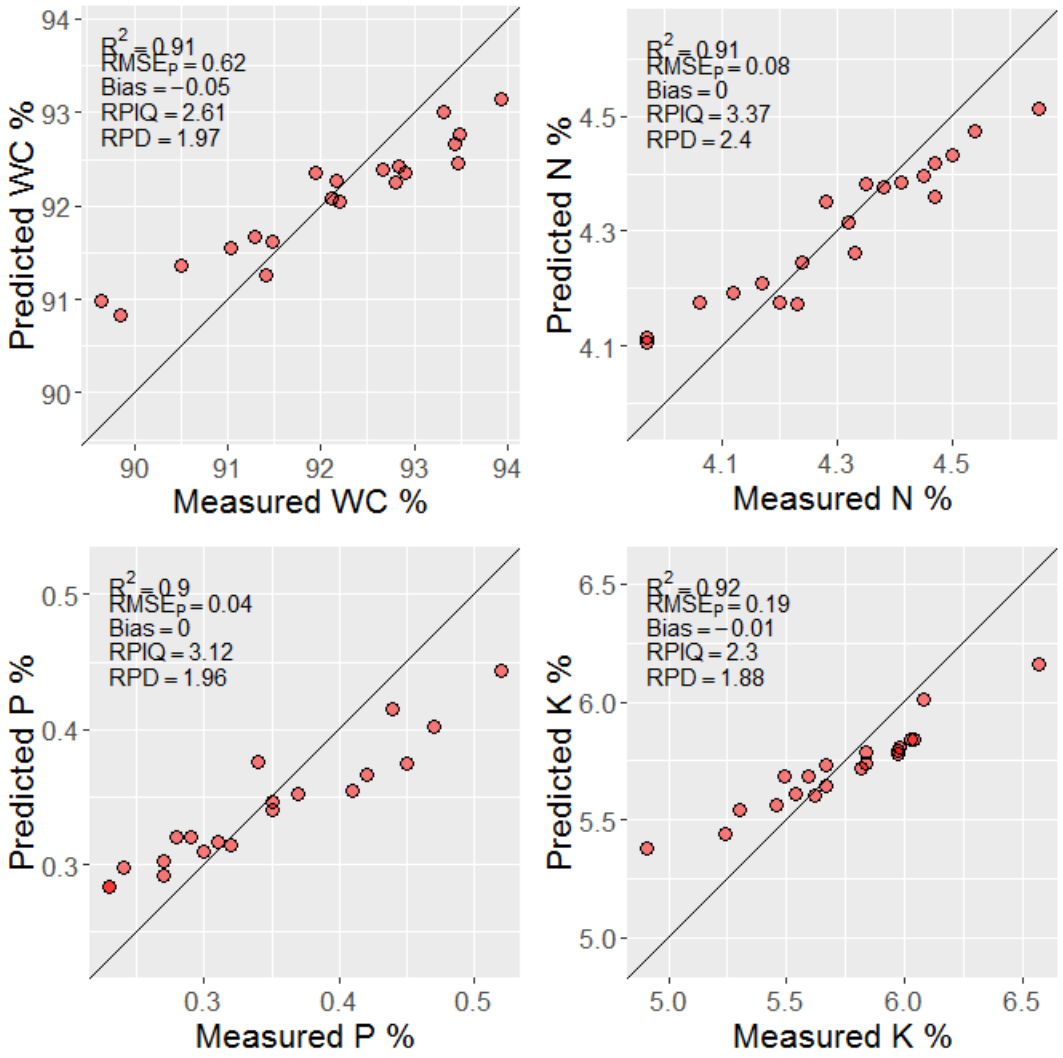

Figure 3.4. Scattered plots of predicted vs. measured values of WC, N, P and K using Random Forest.

Table 3.3. Cross validation results for predicting plant WC, N, P and K using four different modeling techniques

Properties Predicted	Modeling Technique	R^2	RMSE	RPD
Water Content	PLS	0.07	1.15	1.06
	ANN	0.06	1.18	1.04
	RF	0.91	0.62	1.97
	SVR	0.51	0.87	1.41
Nitrogen	PLS	0.5	0.13	1.45
	ANN	0.19	0.17	1.11
	RF	0.91	0.08	2.4
	SVR	0.74	0.1	1.79
Phosphorous	PLS	0.1	0.08	1.08
	ANN	0.1	0.08	1.03
	RF	0.9	0.04	1.96
	SVR	0.05	0.08	1.01
Potassium	PLS	0.02	0.35	1.04
	ANN	0.01	0.36	1.03
	RF	0.92	0.19	1.88
	SVR	0.1	0.35	1.04

consequently could not be used for the prediction of new samples, they do tend to show the possibility of obtaining 3D spectral point clouds for the prediction of biochemical properties in the plant non-destructively. In addition, with further data processing, there is also the possibility of deriving structural properties of the plants from the 3D point cloud obtained through structure from motion. Zia et al. (2013) reconstructed the 3D model of different solid structures using hyperspectral images. Despite its potential application in plant phenotyping, 3D reconstruction in plant phenotyping using hyperspectral images is very rare. Instead of capturing the images at different bands separately, we could use a hyperspectral camera to capture plant images at once for a large number of narrow hyperspectral bands and use those images to construct 3D point clouds at all these bands. We believe that these types of 3D hyperspectral point clouds would be more realistic representation of plants containing both the morphological and the biochemical information.

3.4 CONCLUSION

This chapter presents a method of obtaining multispectral point clouds using 2D images taken at different narrow spectral bands using structure from motion technique. An experiment was conducted to generate the spectral point clouds of maize plants at seven different bands. The possibility of deriving the water content and nutrient content (N, P and K) from the spectral point cloud was investigated using four different modeling techniques: Partial Least Squares Regression, Artificial Neural Networks, Random Forest and Support Vector Regression. Random Forest performed consistently better in predicting all the four response variables (with $R^2 \geq 0.9$) and thus demonstrated the possibility of deriving biochemical properties of the plants from the 3D spectral point clouds.

CHAPTER 4

CONCLUSION

There were two major objectives of the study. The first was to generate a 3D point cloud of maize and sorghum plants to quantify the morphological properties; and the second was to obtain a spectral point cloud for inferring the biochemical properties of maize plants.

For the first part, a 2D scanning LiDAR in combination with a turntable was used to generate a 3D point cloud of maize and sorghum which was then used to derive the structural parameters of interest. The non-destructive measurement by the LiDAR showed satisfactory results for estimating the three important structural parameters: leaf area, leaf inclination angle and leaf angular distribution. Also, with the entire 3D point cloud in hand, numerous other plant properties like plant height, plant biomass, leaf length, leaf width etc. can be derived. Since LiDAR gives distance values in real time, it is suitable to generate the point clouds of the crops in a high throughput fashion. The study showed that there is a potential of using such technique in the high throughput measurement systems, particularly in the automated greenhouses, to measure hundreds of plants per day nondestructively with high accuracy.

For the second objective, Structure from Motion technique was applied to generate the spectral point cloud of the maize plants from a number of 2D images taken at various narrow wavelength bands (10 nm). The spectral curve obtained from the multispectral point cloud resembled a typical plant spectral signature. The prediction of the nitrogen, phosphorous, potassium and water content using random forest showed the possibility of using spectral point clouds in combination with a modelling technique to derive the biochemical properties of the plants.

Moving further, there is an avenue for deriving the morphological parameters along

with the biochemical properties either by entirely using structure from motion technique or by registering morphological data from the LiDAR with the spectral information derived using some other techniques (hyperspectral imaging, spectroscopy). Such types of 3D plant models with the narrow-band spectral information over a wide spectral range would be a more holistic representation of the real-world plants and greatly enhance phenotyping capacities.

REFERENCES

Alenyà, G., Dellen, B., & Torras, C. (2011). 3D modelling of leaves from color and ToF data for robotized plant measuring. *Proceedings - IEEE International Conference on Robotics and Automation*, 3408–3414. doi:10.1109/ICRA.2011.5980092

Azzari, G., Goulden, M. L., & Rusu, R. B. (2013). Rapid characterization of vegetation structure with a microsoft kinect sensor. *Sensors (Switzerland)*, *13*(2), 2384–2398. doi:10.3390/s130202384

Biskup, B., Scharr, H., Schurr, U., & Rascher, U. (2007). A stereo imaging system for measuring structural parameters of plant canopies. *Plant, Cell and Environment*, *30*(10), 1299–1308. doi:10.1111/j.1365-3040.2007.01702.x

Campbell, G. S., & Norman, J. M. (2012). *An Introduction to Environmental Biophysics*. Springer Science & Business Media.

Campbell, M. T., Knecht, A. C., Berger, B., Brien, C. J., Wang, D., & Walia, H. (2015). Integrating Image-Based Phenomics and Association Analysis to Dissect the Genetic Architecture of Temporal Salinity Responses in Rice. *Plant Physiology*, *168*(4), 1476–1489. doi:10.1104/pp.15.00450

Campolide, C. D. (2007). 3D Surface Modelling of Tomato Plants Using Close-Range. *Europe*, *1*(2001).

Carins Murphy, M. R., Jordan, G. J., & Brodribb, T. J. (2012). Differential leaf expansion can enable hydraulic acclimation to sun and shade. *Plant, Cell and Environment*, *35*(8), 1407–1418. doi:10.1111/j.1365-3040.2012.02498.x

Chen, Y., Zhang, W., Yan, K., Li, X., & Zhou, G. (2012). Extracting corn geometric structural parameters using Kinect. *International Geoscience and Remote Sensing Symposium (IGARSS)*, 6673–6676. doi:10.1109/IGARSS.2012.6352068

Chéné, Y., Rousseau, D., Lucidarme, P., Bertheloot, J., Caffier, V., Morel, P., … Chapeau-Blondeau, F. (2012). On the use of depth camera for 3D phenotyping of entire plants. *Computers and Electronics in Agriculture*, *82*, 122–127. doi:10.1016/j.compag.2011.12.007

Cignoni, P., Callieri, M., Corsini, M., Dellepiane, M., Ganovelli, F., & Ranzuglia, G. (2008). MeshLab: an Open-Source Mesh Processing Tool. In V. Scarano, R. D. Chiara, & U. Erra (Eds.), *Eurographics italian chapter conference*. doi:10.2312/LocalChapterEvents/ItalChap/ItalianChapConf2008/129-136

Dauzat, J., Rapidel, B., & Berger, A. (2001). Simulation of leaf transpiration and sap flow in virtual plants: Model description and application to a coffee plantation in Costa Rica. *Agricultural and Forest Meteorology*, *109*(2), 143–160. doi:10.1016/S0168-1923(01)00236-2

De Wit, C. T. (1965). Photosynthesis of leaf Canopies. *Analysis*, (April), 11–19.

Duran, C., Appleby, N., Vardy, M., Imelfort, M., Edwards, D., & Batley, J. (2009). Single nucleotide polymorphism discovery in barley using autoSNPdb. *Plant Biotechnology Journal*, *7*(4), 326–333. doi:10.1111/j.1467-7652.2009.00407.x

Easlon, H. M., & Bloom, A. J. (2014). Easy Leaf Area: Automated Digital Image Analysis for Rapid and Accurate Measurement of Leaf Area. *Applications in Plant Sciences*, *2*(7), 1400033. doi:10.3732/apps.1400033

Eitel, J. U. H., Magney, T. S., Vierling, L. A., Brown, T. T., & Huggins, D. R. (2014). LiDAR based biomass and crop nitrogen estimates for rapid, non-destructive

assessment of wheat nitrogen status. *Field Crops Research*, *159*, 21–32. doi:10.1016/j.fcr.2014.01.008

Fahlgren, N., Gehan, M. A., & Baxter, I. (2015). Lights, camera, action: High-throughput plant phenotyping is ready for a close-up. *Current Opinion in Plant Biology*, *24*, 93–99. doi:10.1016/j.pbi.2015.02.006

Fang, F. (2015). The Retrieval of Leaf Inclination Angle and Leaf Area Index in Maize, 76.

Fiorani, F., & Schurr, U. (2013). Future scenarios for plant phenotyping. *Annual review of plant biology*, *64*, 267–291.

Freeman, K. W., Girma, K., Arnall, D. B., Mullen, R. W., Martin, K. L., Teal, R. K., & Raun, W. R. (2007). By-plant prediction of corn forage biomass and nitrogen uptake at various growth stages using remote sensing and plant height. *Agronomy Journal*, *99*(2), 530–536. doi:10.2134/agronj2006.0135

Friedli, M., Kirchgessner, N., Grieder, C., Liebisch, F., Mannale, M., & Walter, A. (2016). Terrestrial 3D laser scanning to track the increase in canopy height of both monocot and dicot crop species under field conditions. *Plant Methods*, *12*(1), 1–15. doi:10.1186/s13007-016-0109-7

Furbank, R. T., & Tester, M. (2011). Phenomics - technologies to relieve the phenotyping bottleneck. *Trends in Plant Science*, *16*(12), 635–644. doi:10.1016/j.tplants.2011.09.005

Furness, G. O., Magarey, P. A., Miller, P. M., & Drew, H. J. (1998). Fruit tree and vine sprayer calibration based on canopy size and length of row: Unit canopy row method. *Crop Protection*, *17*(8), 639–644. doi:10.1016/S0261-2194(98)00064-7

Ge, Y., Bai, G., Stoerger, V., & Schnable, J. C. (2016). Temporal dynamics of maize plant growth, water use, and leaf water content using automated high throughput RGB

and hyperspectral imaging. *Computers and Electronics in Agriculture*, *127*, 625–632. doi:10.1016/j.compag.2016.07.028

Gibbs, J. A., Pound, M., Wells, D. M., Murchie, E., French, A., & Pridmore, T. (2015). Three-Dimensional Reconstruction of Plant Shoots from Multiple Images using an Active Vision System. *G. Kootstra, Y Edan, E van Henten, and M Bergerman (Eds.), Proceedings of the IROS Workshop on Agri-Food Robotics*.

Glasbey, C. A., Polder, G., Heijden, G. W., & Song, Y. (2014a). Non-destructive automatic leaf area measurements by combining stereo and time-of-flight images. *IET Computer Vision*, *8*(5), 391–403. doi:10.1049/iet-cvi.2013.0056

Glasbey, C. A., Polder, G., Heijden, G. W., & Song, Y. (2014b). Non-destructive automatic leaf area measurements by combining stereo and time-of-flight images. *IET Computer Vision*, *8*(5), 391–403. doi:10.1049/iet-cvi.2013.0056

Goel, N. S., & Strebel, D. E. (1984). Simple Beta Distribution Representation of Leaf Orientation in Vegetation Canopies1. *Agronomy Journal*, *76*(5), 800. doi:10.2134/agronj1984.00021962007600050021x

Golbach, F., Kootstra, G., Damjanovic, S., Otten, G., & van de Zedde, R. (2016). Validation of plant part measurements using a 3D reconstruction method suitable for high-throughput seedling phenotyping. *Machine Vision and Applications*, *27*(5), 663–680. doi:10.1007/s00138-015-0727-5

Golzarian, M. R., Frick, R. A., Rajendran, K., Berger, B., Roy, S., Tester, M., & Lun, D. S. (2011). Accurate inference of shoot biomass from high-throughput images of cereal plants. *Plant Methods*, *7*(1), 2. doi:10.1186/1746-4811-7-2

Goudriaan, J. (1988). The bare bones of leaf-angle distribution in radiation models for canopy photosynthesis and energy exchange. *Agricultural and Forest Meteorology*, *43*(2), 155–169. doi:10.1016/0168-1923(88)90089-5. arXiv: 1504.0596

Goudriaan, J., & Laar, H. V. (2012). *Modelling Potential Crop Growth Processes: Textbook with Exercises* (Vol. 2). Springer Science & Business Media.

Hakala, T., Suomalainen, J., Kaasalainen, S., & Chen, Y. (2012). Full waveform hyperspectral LiDAR for terrestrial laser scanning. *Optics Express*, *20*(7), 7119. doi:10.1364/OE.20.007119

Hanan, J. (1997). Virtual plants - Integrating architectural and physiological models. *Environmental Modelling and Software*, *12*(1), 35–42. doi:10.1016/S1364-8152(96)00040-0

Hirose, T. (2005). Development of the Monsi-Saeki theory on canopy structure and function. *Annals of Botany*, *95*(3), 483–494. doi:10.1093/aob/mci047

Jiang, Y., Li, C., & Paterson, A. H. (2016). High throughput phenotyping of cotton plant height using depth images under field conditions. *Computers and Electronics in Agriculture*, *130*, 57–68. doi:10.1016/j.compag.2016.09.017

Jimenez-Berni, J. A., Deery, D. M., Rozas-Larraondo, P., Condon, A. (G., Rebetzke, G. J., James, R. A., … Sirault, X. R. R. (2018). High Throughput Determination of Plant Height, Ground Cover, and Above-Ground Biomass in Wheat with LiDAR. *Frontiers in Plant Science*, *9*(February), 1–18. doi:10.3389/fpls.2018.00237

Jones, Coops, N. C., & Sharma, T. (2010). Assessing the utility of airborne hyperspectral and LiDAR data for species distribution mapping in the coastal Pacific Northwest, Canada. *Remote Sensing of Environment*, *114*(12), 2841–2852. doi:10.1016/j.rse.2010.07.002

Jones, & Vaughan, R. A. (2010). *Remote Sensing of Vegetation: Principles, Techniques, and Applications*. Oxford University Press.

Juneau, K. J., & Tarasoff, C. S. (2012). Leaf area and water content changes after permanent and temporary storage. *PLoS ONE*, *7*(8), 1–6. doi:10.1371/journal.pone.0042604

Karnieli, A., Agam, N., Pinker, R. T., Anderson, M., Imhoff, M. L., Gutman, G. G., … Goldberg, A. (2010). Use of NDVI and land surface temperature for drought assessment: Merits and limitations. *Journal of Climate*, *23*(3), 618–633. doi:10.1175/2009JCLI2900.1

Kazmi, W., Foix, S., Alenyà, G., & Andersen, H. J. (2014). Indoor and outdoor depth imaging of leaves with time-of-flight and stereo vision sensors: Analysis and comparison. *ISPRS Journal of Photogrammetry and Remote Sensing*, *88*, 128–146. doi:10.1016/j.isprsjprs.2013.11.012

Klukas, C., Chen, D., & Pape, J.-M. (2014). Integrated Analysis Platform: An Open-Source Information System for High-Throughput Plant Phenotyping. *Plant Physiology*, *165*(2), 506–518. doi:10.1104/pp.113.233932

Kumar, P., Cai, J., & Miklavcic, S. (2013). 3D Reconstruction , Modelling and Analysis of in Situ Root System Architecture. *20th International Congress on Modelling and Simulation*, (December), 1–6.

Larcher, W. (2003). *Physiological plant ecology: ecophysiology and stress physiology of functional groups*. Springer Science & Business Media.

Li, L., Zhang, Q., & Huang, D. (2014). A review of imaging techniques for plant phenotyping. *Sensors (Switzerland)*, *14*(11), 20078–20111. doi:10.3390/s141120078

Lin, Y. (2015). LiDAR: An important tool for next-generation phenotyping technology of high potential for plant phenomics? *Computers and Electronics in Agriculture*, *119*, 61–73. doi:10.1016/j.compag.2015.10.011

Liu, W. T., & Negrón Juárez, R. I. (2001). ENSO drought onset prediction in northeast Brazil using NDVI. *International Journal of Remote Sensing*, *22*(17), 3483–3501. doi:10.1080/01431160010006430

Liu, Acosta-Gamboa, L., Huang, X., & Lorence, A. (2017). Novel Low Cost 3D Surface Model Reconstruction System for Plant Phenotyping. *Journal of Imaging*, *3*(3), 39. doi:10.3390/jimaging3030039

Lu, S., Zhao, H., Des Marais, D. L., Parsons, E. P., Wen, X., Xu, X., … Jenks, M. A. (2012). Arabidopsis ECERIFERUM9 Involvement in Cuticle Formation and Maintenance of Plant Water Status. *Plant Physiology*, *159*(3), 930–944. doi:10.1104/pp.112.198697

Ma, B. L., Morrison, M. J., & Dwyer, L. M. (1996). Canopy light reflectance and field greenness to assess nitrogen fertilization and yield of maize. *Agronomy Journal*, *88*(6), 915–920. doi:10.2134/agronj1996.00021962003600060011x

Madec, S., Baret, F., de Solan, B., Thomas, S., Dutartre, D., Jezequel, S., … Comar, A. (2017). High-Throughput Phenotyping of Plant Height: Comparing Unmanned Aerial Vehicles and Ground LiDAR Estimates. *Frontiers in Plant Science*, *8*(November), 1–14. doi:10.3389/fpls.2017.02002

Mccormick, R. F., Truong, S. K., & Mullet, J. E. (2016). 3D sorghum reconstructions from depth images identify QTL regulating shoot architecture. *Plant Physiology*, pp.00948.2016. doi:10.1104/pp.16.00948

Mikhnevich, M., & Hébert, P. (2011). Shape from silhouette under varying lighting and multi-viewpoints. *Proceedings - 2011 Canadian Conference on Computer and Robot Vision, CRV 2011*, 285–292. doi:10.1109/CRV.2011.45

Miller, E. C. (1938). *Plant Physiology, with Reference to the Green Plant, by Edwin C. Miller...* McGraw-Hill Book Company, Incorporated.

Nguyen, C. V., Fripp, J., Lovell, D. R., Furbank, R., Kuffner, P., Daily, H., & Sirault, X. (2016). 3D Scanning System for Automatic High-Resolution Plant Phenotyping. *2016 International Conference on Digital Image Computing: Techniques and Applications, DICTA 2016*. doi:10.1109/DICTA.2016.7796984

Nguyen, T. T., Slaughter, D. C., Max, N., Maloof, J. N., & Sinha, N. (2015). Structured light-based 3D reconstruction system for plants. *Sensors (Switzerland)*, *15*(8), 18587–18612. doi:10.3390/s150818587

Nicotra, A. B., Leigh, A., Boyce, C. K., Jones, C. S., Niklas, K. J., Royer, D. L., & Tsukaya, H. (2011). The evolution and functional significance of leaf shape in the angiosperms. *Functional Plant Biology*, *38*(7), 535–552. doi:10.1071/FP11057

Nobel, P. S., Forseth, I. N., & Long, S. P. (1993). Canopy structure and light interception. In D. O. Hall, J. M. O. Scurlock, H. R. Bolhàr-Nordenkampf, R. C. Leegood, & S. P. Long (Eds.), *Photosynthesis and production in a changing environment: A field and laboratory manual* (pp. 79–90). doi:10.1007/978-94-011-1566-7_6

Pandey, P., Ge, Y., Stoerger, V., & Schnable, J. C. (2017). High Throughput In vivo Analysis of Plant Leaf Chemical Properties Using Hyperspectral Imaging. *Frontiers in Plant Science*, *8*(August), 1–12. doi:10.3389/fpls.2017.01348

Paproki, A., Sirault, X. R. R., Berry, S., Furbank, R. T., & Fripp, J. (2012). A novel mesh processing based technique for 3D plant analysis. *BMC Plant Biology*, *12*(1), 63. doi:10.1186/1471-2229-12-63

Passioura, J. (2012). Phenotyping for drought tolerance in grain crops: When is it useful to breeders? *Functional Plant Biology*, *39*(11), 851–859.

Paulus, S., Behmann, J., Mahlein, A. K., Plümer, L., & Kuhlmann, H. (2014). Low-cost 3D systems: Suitable tools for plant phenotyping. *Sensors (Switzerland)*, *14*(2), 3001–3018. doi:10.3390/s140203001

Paulus, S., Schumann, H., Kuhlmann, H., & Léon, J. (2014). High-precision laser scanning system for capturing 3D plant architecture and analysing growth ofcereal plants. *Biosystems Engineering*, *121*, 1–11. doi:10.1016/j.biosystemseng.2014.01.010

Pendleton, J. W., Smith, G. E., Winter, S. R., & Johnston, T. J. (1968). Field Investigations of the Relationships of Leaf Angle in Corn (Zea mays L.) to Grain Yield and Apparent Photosynthesis1. *Agronomy Journal*, *60*(4), 422. doi:10.2134/agronj1968.00021962006000040027x

Poehlman, J. M., Sleper, D. A., & Rudd, J. (1995). *Breeding field crops*. Springer.

Pons, T. L., Lambers, H., & Chapin III, F. S. (1998). Plant physiological ecology. Springer, New York.

Pound, M. P., French, A. P., Murchie, E. H., & Pridmore, T. P. (2014). Automated Recovery of Three-Dimensional Models of Plant Shoots from Multiple Color Images. *Plant Physiology*, *166*(4), 1688–1698. doi:10.1104/pp.114.248971

Puttonen, E., Jaakkola, A., Litkey, P., & Hyyppä, J. (2011). Tree classification with fused mobile laser scanning and hyperspectral data. *Sensors*, *11*(5), 5158–5182. doi:10.3390/s110505158

Reynolds, M. P., van Ginkel, M., & Ribaut, J. (2000). Avenues for genetic modification of radiation use efficiency in wheat. *Journal of Experimental Botany*, *51*(suppl_1), 459–473. doi:10.1093/jexbot/51.suppl_1.459

Robert, C., Fournier, C., Andrieu, B., & Ney, B. (2008). Coupling a 3D virtual wheat (Triticum aestivum) plant model with a Septoria tritici epidemic model (Septo3D): A new approach to investigate plant-pathogen interactions linked to canopy architecture. *Functional Plant Biology*, *35*(10), 997–1013. doi:10.1071/FP08066

Ross, J. (1981). *The radiation regime and architecture of plant stands*. Dr W. Junk Publishers.

Santos, T. T., & De Oliveira, A. A. (2012). Image-based 3D digitizing for plant architecture analysis and phenotyping. *Workshop on Industry Applications*, *2012*, 21–28. doi:10.13140/2.1.4576.1608

Siegfried, W., Viret, O., Huber, B., & Wohlhauser, R. (2007). Dosage of plant protection products adapted to leaf area index in viticulture. *Crop Protection*, *26*(2), 73–82. doi:10.1016/j.cropro.2006.04.002

Sinoquet, H., Le Roux, X., Adam, B., Ameglio, T., & Daudet, F. (2001). RATP a model for simulating the spatial distribution of radiation absortion traspiratons and photosynthesis within canopies. *Plant, Cell and Environment*, *24*, 395–406.

Stewart, D. W., & Dwyer, L. M. (1999). Mathematical characterisation of leaf shape and area in maize hybrids. *Crop Sciences*, *39*, 422–427.

Strable, J., Wallace, J. G., Unger-Wallace, E., Briggs, S., Bradbury, P., Buckler, E. S., & Vollbrecht, E. (2017). Maize YABBY Genes drooping leaf1 and drooping leaf2 Regulate Plant Architecture. *The Plant Cell*, *29*(July), tpc.00477.2016. doi:10.1105/tpc.16.00477

Strothmann, W., Ruckelshausen, A., & Hertzberg, J. (2014). Multi-wavelength laser line profile sensing for agricultural crop characterization. *Proceedings of SPIE Vol. 9141: Optical Sensing and Detection III. SPIE Photonics Europe (SPIE-2014), April 14-17*, *Vol. 9141*, 1–14. doi:10.1117/12.2052009

Sun, S., Li, C., & Paterson, A. H. (2017). In-field high-throughput phenotyping of cotton plant height using LiDAR. *Remote Sensing*, *9*(4), 1–21. doi:10.3390/rs9040377

Tardieu, F. (2003). Virtual plants: Modelling as a tool for the genomics of tolerance to water deficit. *Trends in Plant Science*, *8*(1), 9–14. doi:10.1016/S1360-1385(02)00008-0

Thapa, S., Zhu, F., Walia, H., Yu, H., & Ge, Y. (2018). A novel LiDAR-Based instrument for high-throughput, 3D measurement of morphological traits in maize and sorghum. *Sensors (Switzerland)*, *18*(4). doi:10.3390/s18041187

Thomas, V., McCaughey, J. H., Treitz, P., Finch, D. A., Noland, T., & Rich, L. (2009). Spatial modelling of photosynthesis for a boreal mixedwood forest by integrating micrometeorological, lidar and hyperspectral remote sensing data. *Agricultural and Forest Meteorology*, *149*(3-4), 639–654. doi:10.1016/j.agrformet.2008.10.016

Tremblay, N., Wang, Z., Ma, B. L., Belec, C., & Vigneault, P. (2009). A comparison of crop data measured by two commercial sensors for variable-rate nitrogen application. *Precision Agriculture*, *10*(2), 145–161. doi:10.1007/s11119-008-9080-2

Truong, S. K., McCormick, R. F., Rooney, W. L., & Mullet, J. E. (2015). Harnessing genetic variation in leaf angle to increase productivity of sorghum bicolor. *Genetics*, *201*(3), 1229–1238. doi:10.1534/genetics.115.178608

Vos, J., Evers, J. B., Buck-Sorlin, G. H., Andrieu, B., Chelle, M., & De Visser, P. H. (2010). Functional-structural plant modelling: A new versatile tool in crop science. *Journal of Experimental Botany*, *61*(8), 2101–2115. doi:10.1093/jxb/erp345

Warman, L., Moles, A. T., & Edwards, W. (2011). Not so simple after all: Searching for ecological advantages of compound leaves. *Oikos*, *120*(6), 813–821. doi:10.1111/j.1600-0706.2010.19344.x

Wehr, A., & Lohr, U. (1999). Airborne laser scanning—an introduction and overview. *ISPRS Journal of Photogrammetry & Remote Sensing*, *54*, 68–82. doi:Doi:10.1016/s0924-2716(99)00011-8

Wei, G., Shalei, S., Bo, Z., Shuo, S., Faquan, L., & Xuewu, C. (2012). Multi-wavelength canopy LiDAR for remote sensing of vegetation: Design and system performance. *ISPRS Journal of Photogrammetry and Remote Sensing*, *69*, 1–9. doi:10.1016/j.isprsjprs.2012.02.001

Wilson, P. A., & Chakrabrty, S. (1998). The virtual plant: A new tool for the study and management of plant diseases. *Crop Protection*, *17*(3), 231–239. doi:10.1016/S0261-2194(97)00088-4

Wu, C. (2018). Towards Linear-time Incremental Structure from Motion. *IEEE Transactions on Signal and Information Processing over Networks*. doi:10.1109/TSIPN.2018.2854669

Yamamoto, S., Hayashi, S., Saitoh, S., Ochiai, Y., Tsubota, S., Takeshima, Y., … Saga, K. (2013). Basic study on non-destructive growth measurement of strawberry plants

using a machine-vision system. In *International symposium on new technologies for environment control, energy-saving and crop production in greenhouse and plant 1037* (pp. 651–656).

Yengoh, G. T., Dent, D., Olsson, L., Tengberg, A. E., & Tucker, C. J. (2016). Applications of NDVI for Land Degradation Assessment BT - Use of the Normalized Difference Vegetation Index (NDVI) to Assess Land Degradation at Multiple Scales: Current Status, Future Trends, and Practical Considerations. In G. T. Yengoh, D. Dent, L. Olsson, A. E. Tengberg, & C. J. Tucker III (Eds.), (pp. 17–25). doi:10.1007/978-3-319-24112-8_3

Zanten, M., Pons, T. L., Janssen, J. A., Voesenek, L. A., & Peeters, A. J. (2010). On the relevance and control of leaf angle. *Critical Reviews in Plant Sciences*, *29*(5), 300–316. doi:10.1080/07352689.2010.502086